Space Science Reviews (2023) 219:29
https://doi.org/10.1007/s11214-023-00966-y

Resurfacing History and Volcanic Activity of Venus

Robert R. Herrick[1] · Evan T. Bjonnes[2] · Lynn M. Carter[3] · Taras Gerya[4] · Richard C. Ghail[5] · Cédric Gillmann[6,4] · Martha Gilmore[7] · Scott Hensley[8] · Mikhail A. Ivanov[9] · Noam R. Izenberg[10] · Nils T. Mueller[11] · Joseph G. O'Rourke[12] · Tobias Rolf[13,14] · Suzanne E. Smrekar[8] · Matthew B. Weller[2,15]

Received: 28 June 2022 / Accepted: 1 March 2023 / Published online: 25 April 2023

Abstract
Photogeologic principles can be used to suggest possible sequences of events that result in the present planetary surface. The most common method of evaluating the absolute age of a planetary surface remotely is to count the number of impact craters that have occurred after the surface formed, with the assumption that the craters occur in a spatially random fashion over time. Using additional assumptions, craters that have been partially modified by later geologic activity can be used to assess the time frames for an interpreted sequence of events. The total number of craters on Venus is low and the spatial distribution taken by itself is nearly indistinguishable from random. The overall implication is that the Venusian surface is much closer to Earth in its youthfulness than the other, smaller inner solar system bodies. There are differing interpretations of the extent to which volcanism and tectonics have modified the craters and of the regional and global sequences of geologic events. Consequently, a spectrum of global resurfacing views has emerged. These range from a planet that has evolved to have limited current volcanism and tectonics concentrated in a few zones to a planet with Earth-like levels of activity occurring everywhere at similar rates but in different ways. Analyses of the geologic record have provided observations that are challenging to reconcile with either of the endmember views. The interpretation of a global evolution with time in the nature of geologic activity relies on assumptions that have been challenged, but there are other observations of areally extensive short-lived features such as canali that are challenging to reconcile with a view of different regions evolving independently. Future data, especially high-resolution imaging and topography, can provide the details to resolve some of the issues. These different global-evolution viewpoints must tie to assessments of present-day volcanic and tectonic activity levels that can be made with the data from upcoming missions.

Keywords Venus · Venus volcanism · Venus geology · Venus resurfacing history

Venus: Evolution Through Time
Edited by Colin F. Wilson, Doris Breuer, Cédric Gillmann, Suzanne E. Smrekar, Tilman Spohn and Thomas Widemann

Extended author information available on the last page of the article

1 Introduction

At minimum, it will be a few decades before samples from the Venusian surface can be dated in situ or returned to Earth for analysis. Understanding the volcanic and tectonic history of the planet thus involves primarily two types of activities: determining sequences of events on the surface by applying photogeologic analysis techniques to synthetic aperture radar (SAR) images, and evaluating the age of surfaces by assuming that impact cratering of the surface occurs in a spatially random manner with a known frequency so that craters can be used as a crude clock.

Dating the very last activity that occurred on a surface can be accomplished by counting the number of craters that occurred after that activity ceased. As we discuss below, using modeling and certain assumptions, craters that do not postdate all geologic activity can provide information about the ages of the events that altered the craters (e.g., post-impact faulting or partial volcanic filling). The timing, pattern, and nature of observed geologic events and accompanying crater alteration provide critical clues about the global geodynamic scenarios that have led to the current geomorphology. Other articles in this collection delve into the details of volcanism and deformation and the geodynamic models that have driven resurfacing. In this article we concern ourselves with efforts to calibrate the cratering clock, our understanding of how and where craters have been altered since formation, and attempts to determine the parameter space of acceptable geomorphic models for global resurfacing that are consistent with observations. Unfortunately, the combination of a relatively young surface and atmospheric filtering of small meteoroids means that Venus has far fewer impact craters than Mars, Mercury, or Earth's moon, making the job particularly difficult.

We begin (Sect. 2) by reviewing estimates of the rate at which impact craters form on the surface, the first step in using the cratering record to understand the history of Venus. A remarkable observation from the initial results of the Magellan mission was that the distribution of craters, taken alone, was nearly indistinguishable from a random distribution. We devote a section to a statistical assessment of the pattern of craters and its relationship to the global pattern of geomorphologic units (Sect. 3). We then discuss the general ways in which craters get altered by subsequent geologic processes (Sect. 4). Two- and three-dimensional global models of crater emplacement and volcano/tectonic resurfacing have been developed that attempt to match broad-brush characterizations of global crater modification states (Sect. 5). The overall relationships between craters and different surface features have led to a few end-member models for global geologic surface activity, and we review these unifying concepts (Sect. 6). Some of these concepts involve a present-day level of volcanic and tectonic activity much lower than present-day Earth, while others postulate a level as high or higher. Consequently, we add sub-sections discussing evidence of young and present-day volcanism (Sect. 7). We also include a section (Sect. 8) of miscellaneous geologic observations that provide additional constraints on the global resurfacing history.

The article concludes with an overview of the big-picture models for the planet's geologic history and a summary of how well these ideas mesh with the models and observations presented here. Suggestions for future data collection that can be used to assess these models is provided.

2 Constraints on the Production Rate of Craters

Because we currently have no capability to radioactively date rocks on the surface of Venus, our primary constraint on the absolute age of the Venusian surface comes from using the

impact cratering record as a calendar. The starting assumption is that craters form in a spatially random pattern over time with a rate that is constant or slowly changing with time, and a size-frequency distribution that can be fit with a smooth curve. There are three basic components to understanding how frequently craters of a specified size form on Venus: 1) knowledge of the velocities and size-frequency distribution of objects entering the Venusian atmosphere; 2) understanding of how the Venusian atmosphere affects those objects; and 3) for those objects that reach the surface, knowledge of the size of impact crater produced. In general terms, one of two approaches are used to solve for 1) and 3) as if Venus were an airless body, and then craters on "atmosphere-free Venus" are convolved with a model of how the atmosphere filters projectiles and modifies crater formation. Estimates of the three components are used to determine a crater production function, or the size-frequency distribution of craters for a surface of a specified area and age.

The first approach to estimating crater production on an airless Venus is to take the size-frequency distribution of lunar craters, which have been calibrated by dating lunar samples for selected areas, and attempt to translate those curves to Venus. The knowledge required is the rate of impact on Venus relative to the moon and how large a crater on Venus would be relative to the same-sized crater on the moon. Impacts on both bodies come from a mix of asteroids, short-period comets, and long-period comets, and the relative numbers and proportions of these categories differ between bodies. Relative crater size for a given impactor on the two bodies is a function of primarily planetary gravity, impact velocity, and impactor density. Thus, a crater scaling law must be identified and applied, relative impact velocities must be assessed, and impactor densities must be assumed. A problem with using the lunar curve for Venus is that the latter has a much younger surface than the most confidently calibrated lunar curves, which date to formation of the lunar maria 3+ Ga; a constant or slowly decreasing impact rate over the last 3 Gy is often assumed (e.g., Stöffler et al. 2006).

A second approach to estimating crater production on an airless Venus is to use a present-day census of potential Venus meteoroids, assess their probability of impact, and use a crater scaling law to evaluate likely impact crater size. This approach trades the problem of interpolating the lunar curve from 3 Ga for the problem of assuming that the current observable population of asteroids and comets is representative of the past few hundred My. Also, while the asteroid population is relatively well surveyed at the size range of objects capable of making it through the Venusian atmosphere, populations of short- and long-period comets are less so. Finally, the first approach only requires estimating the relative size of a crater formed under lunar gravity compared to Venusian gravity, while the second approach requires that the absolute size scaling is correct.

Of some of the more widely cited papers with production ages estimates, the post-Venera 15/16 paper by Ivanov et al. (1986) used the first approach, the Magellan-era work of Phillips et al. (1992) compared both approaches, and the second approach was used by Korycansky and Zahnle (2005), McKinnon et al. (1997), Schaber et al. (1992), and Strom et al. (1994). Phillips et al. (1992), Schaber et al. (1992), and Strom et al. (1994) all used estimates of the impactor populations (numbers and proportions of asteroid and comets) by Shoemaker et al. (1991), while McKinnon et al. (1997) developed their own functions that were also used in Korycansky and Zahnle (2005).

The final major hurdle in determining a production age is accounting for the effects of the atmosphere on incoming meteoroids. Meteoroid disruption and deceleration prevent small objects from making it to the surface and forming a crater, while the separation of fragments of other meteoroids results in irregular craters or crater fields (Herrick and Phillips 1994a,b). The end result is that the smallest impact crater on Venus is ~1.5 km across, and the incremental size-frequency distribution rolls over and has reductions relative to the

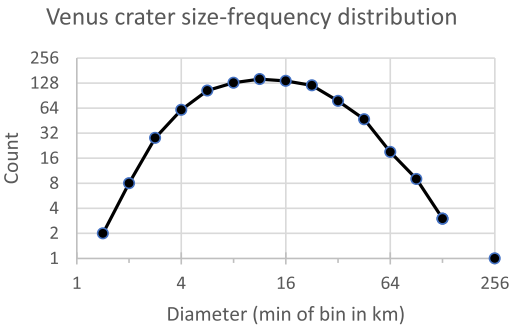

Fig. 1 Size-frequency distribution of certain and probable craters from the database of Herrick et al. (1997). Craters are binned in $\sqrt{2}$ increments of D and plotted at the minimum diameter of the bin. The rollover with decreasing diameter and the lack of craters with D < 1.5 km is attributable to atmospheric filtering of incoming meteoroids

airless body case to crater sizes up to perhaps 30 km in diameter (Herrick and Phillips 1994b; Ivanov et al. 1986; Tauber and Kirk 1976) (Fig. 1). Note that reductions in the size-frequency distribution occur not only from meteoroids not making it to the surface, but also from those that do reach the surface but are slowed and make smaller craters.

The simplest approach to dealing with atmospheric effects is to assume that the straight part of the size-frequency curve, diameter D > ~30 km, is either unaffected by the atmosphere or only affected by a modification of the scaling law to calculate final crater size from an impacting meteoroid; Phillips et al. (1992), and Schaber et al. (1992) consider this approach. Using a small portion of what is already a limited number of craters on Venus to estimate surface age precludes evaluating all but the largest regional differences in surface age. Because different meteoroid types (e.g., iron versus chondritic asteroids, asteroids versus comets) should behave differently in the atmosphere, attempting to match the rollover in the incremental size-frequency distribution not only allows more craters to be used in age calculations, it also constrains the relative proportions of different impactor types. Thus, there have been attempts to match the rollover in the size-frequency curve (Herrick and Phillips 1994b; Ivanov et al. 1986; Korycansky and Zahnle 2005; McKinnon et al. 1997; Phillips et al. 1992) and the number and geometry of craters from clustered impact and crater fields (Herrick and Phillips 1994b; Korycansky and Zahnle 2005). Approaches involve considering meteoroid deceleration that includes flattening (which increases cross-sectional area) and disruption (fragments have larger ratios of surface area to mass), with criteria set for atmospheric explosion (and thus no surface crater) and/or a minimum impact velocity below which a crater is assumed not to form. An important caveat to the curve-fitting studies is an assumption that the shape of the incremental size-frequency distribution is reflective of a production function and that there is no preferential removal of small craters by volcanic or tectonic processes. A never-stated but required assumption of the above studies is that the atmosphere of Venus has not changed in nature over the time of observation; alternatively, the lack of sub-km craters can be seen as evidence that there are no well-preserved areas that formed during a period when Venus had a thin, Earth-like atmosphere.

In short, the range of production ages for the Venusian size-frequency distribution from credible past works spans from ~300-800 Ma, and the spread is mostly due to interpretations of meteoroid flux and crater scaling rather than treatments of atmospheric effects on crater formation. In considering the remainder of this article, it is important to remember that a production age assumes that all of the craters being counted are the last significant thing to have occurred on the surface that they are located. For example, in dating lunar mare deposits, one does not count the craters whose rims poke through the deposit and thus predate it. Furthermore, we cannot use the partially buried craters to date the surface underlying the deposit without some mechanism for determining the number of pre-existing craters that

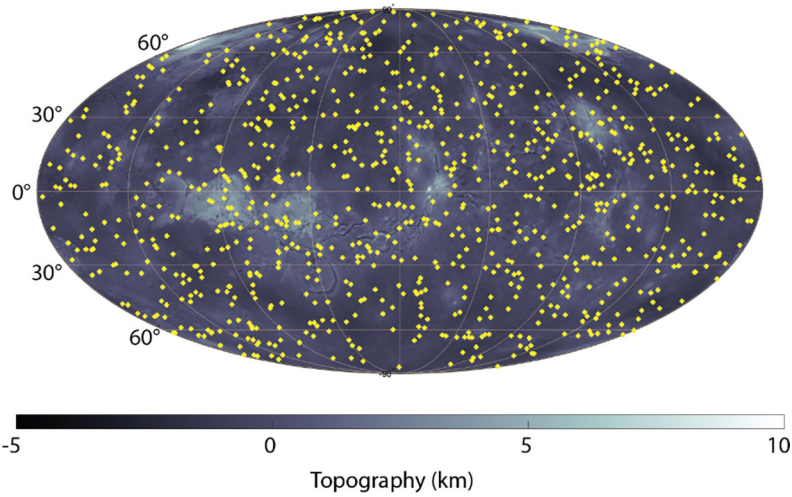

Fig. 2 Global distribution of craters shown by yellow crosses overlaid on Magellan topography. Data shown in Mollweide projection

were completely buried by the deposit. Thus, if the interpretation of Herrick and Rumpf (2011) is correct that 80% or more of craters have experienced post-emplacement partial volcanic modification, then the production age of Venus should be considered to be tens of millions of years, and modeling of surface ages using the entire crater population requires some model of how volcanism buries craters.

3 The Global Pattern of Craters

The distribution and condition of impact craters on a planetary surface can provide insight into how old and geologically active that planet has been through time. Initial results from the Magellan mission indicated that Venus hosts fewer craters than previously expected and these craters are largely unaffected by post-impact erosional, tectonic, or volcanic processes. There are ~900 craters across the surface of Venus with diameters between 1.5 to 270 km (Herrick et al. 1997; Phillips et al. 1992; Schaber et al. 1992). Initial assessments of the Venus crater population showed that all but a few percent of the craters have radar-bright ejecta deposits around most or all of the crater rim, few of the craters have been distorted by tectonic deformation or even have obvious through-going faults, and few of the craters have rims clearly breached by volcanism or volcanically buried central structures (Herrick and Phillips 1994a; Phillips et al. 1992, 1991; Schaber et al. 1992). Based on these observations, it was initially assessed that 80% or more of the craters are pristine (Herrick et al. 1997; Phillips et al. 1992; Schaber et al. 1992), and this was assumed as a constraint for much of the subsequent statistical and modeling work that took place until at least the late 1990s. However, a large portion of these craters have radar-dark floors, suggesting that these craters may have been flooded with lava flows and are not as pristine as previously thought (Herrick and Rumpf 2011; Herrick and Sharpton 2000; O'Rourke et al. 2014).

Maps of impact crater spatial densities can indicate regions of significantly different surface ages because older surfaces have been exposed to impact events for a longer time and, consequently, are predicted to have more craters (Shoemaker and Hackman 1962; Wilhelms

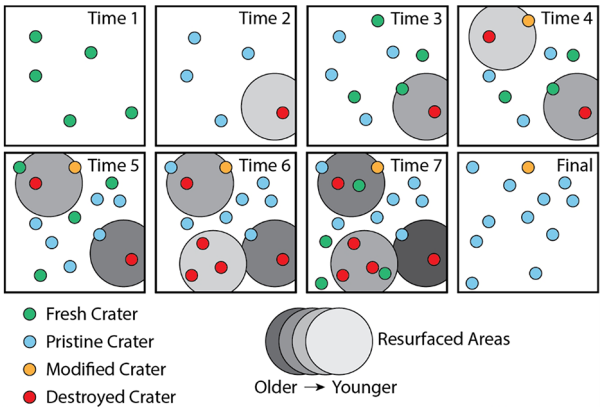

Fig. 3 Schematic illustrating the random crater generation and resurfacing used in Monte Carlo modeling of Venusian crater evolution. Craters which fall on the perimeters of subsequent resurfacing events may be tagged as "Modified" if modification is included as a consideration of the final crater distribution (e.g. Bjonnes et al. 2012), or as "Destroyed" if the analysis does not include modification (e.g. Strom et al. 1994). Because no specific resurfacing mechanism has been identified, final frame shows the modern-day distribution of "pristine" and "modified" craters and omits the resurfaced areas. Figure modified from Bjonnes et al. (2012)

et al. 1987). Crater density maps on Venus reveal that the planet has a distribution of craters across the surface that looks like a set of points placed randomly on a sphere (Fig. 2); in a broad sense, craters are scattered across the surface, but unlike a uniform distribution the inter-crater distance varies and small clusters and gaps occur. This distribution is commonly interpreted as indicating that Venus lacks large areas of notably different ages (Phillips et al. 1992) and instead Venus has a globally-uniform surface age of ~300-800 Ma (McKinnon et al. 1997). One of the main reasons for this conclusion is the low overall number of impact craters on Venus which make it difficult to determine statistically significant regions of variable surface ages. Mapping the global crater distribution against areas with suspected high volcanic activity such as Eastern Aphrodite Terra shows that there is a higher proportion of tectonically deformed or volcanically embayed craters on the margins of areas with lower overall crater densities (Herrick and Phillips 1994a; Phillips et al. 1992; Price and Suppe 1994; Price et al. 1996), and there are some significant differences in crater spatial density between different geomorphologic map units (Kreslavsky et al. 2015; Price and Suppe 1995). That the distribution of small craters is mostly indistinguishable from that of large craters (Phillips et al. 1992; Schaber et al. 1992) places additional constraints on resurfacing processes and has been used to bolster the position that the current crater population is mostly a production function (Strom et al. 1994).

Several studies have used Monte Carlo models to quantify the spatial randomness of impact craters on Venus. Monte Carlo models are a statistical tool used to determine the probability of a certain outcome by generating large datasets of randomized outcomes and determining the probability distribution of the outcomes. Monte Carlo models simulating impact crater distributions on Venus test the spatial randomness of craters emplaced on its surface with or without accompanying simulated resurfacing events (Fig. 3). With a large number of these Monte Carlo models complete, it is possible to generate statistically robust probability distributions of several metrics of spatial randomness, including intercrater angles and nearest-neighbor distances. Some common comparisons between model results and the observed craters are known as probability-probability (P-P) plot and quantile-quantile (Q-Q) plots. P-P plots are a graphical representation of how the cumulative distributions of

two probability functions compare to each other; if two distributions are the same, a P-P plot will be a straight line at 45°. Q-Q plots are similar but instead compare the quantiles of two different datasets, and for identical data, will also plot along a 45° line. The two plots differ in that the centers of probability distributions are more apparent in P-P plots whereas differences in the tails of two distributions are more apparent in Q-Q plots. Observed craters on Venus are statistically indistinguishable from random distributions generated in Monte Carlo models in both P-P and Q-Q plots (Phillips et al. 1992).

Other statistical tests used to compare the existing Venus crater record to simulated distributions are the t-test and chi-squared test. Although similar, a t-test compares two datasets to determine if they are identical and a chi-squared test determines if there is a relationship between two datasets. Strom et al. (1994) tested Venus' crater distribution against Monte Carlo models with and without simulated resurfacing events and determined that the distribution of craters on Venus is indistinguishable from random as determined by both t-tests and chi-squared tests. Before it was realized that most dark floored craters have likely been modified by post-impact volcanism, it was interpreted that the craters on Venus are statistically unlike Monte Carlo simulations with resurfacing patches of 0.001-0.03% of total surface area (too many volcanically modified craters) and 10-50% of total surface area (non-random distribution; Strom et al. 1994). However, impact craters on Venus match both the number of modified craters and their random distribution if resurfaced areas are between 0.1 and 1% of the total surface area if modeled resurfacing events are limited to the first 3 billion years of simulated time (Bjonnes et al. 2012). This conclusion hinges on the timing of volcanic activity; if lava flows between 0.03 – 10% of the total surface area are younger than 3 Ga, then these non-random resurfacing events will remove more craters from the surface than can be recovered by subsequent impact events, resulting in an overall non-random spatial distribution in the present day (Phillips et al. 1992; Romeo and Turcotte 2009).

Although indistinguishable from random when the spatial pattern is considered alone, there is subtle variability within the global distribution of impact craters on Venus. A test of the distance between a crater and its nearest neighbors is more able to determine subtle variability in a global dataset compared to tests which consider the entire probability distribution (Hauck et al. 1998). Testing the mean distance between a crater and its 1st – 4th nearest neighbors reveal that the Venusian plains, which cover 60% of the surface (Ivanov and Head 2011), can be subdivided into up to 4 different units based on morphology, and these morphologic units have statistically significant different mean ages (Hauck et al. 1998). The global crater distribution is also non-random with respect to topography, with a higher-than-expected number of craters located between 6050.9 and 6051.9 km planetary radius (Herrick and Phillips 1994a). Topographic analysis shows a significant crater deficit at planetary radii between 6052.4 and 6052.9 km, an elevation range associated with tectonic rift zones and volcanoes (Herrick and Phillips 1994a).

4 Modification and Degradation of Craters

Most Venusian craters occur in what can generally be called "volcanic plains" (Herrick and Phillips 1994a; Ivanov and Head 2011; Price and Suppe 1995), which is to say that they occur in areas where the terrain is relatively flat and with uniform, low radar backscatter compared to the rough ejecta of an impact crater. The crater population exhibits signs of different degrees of post-impact modification and/or degradation (Herrick and Phillips 1994a; Izenberg et al. 1994; Schaber et al. 1992). Most craters have a circular platform, and continuous ejecta that appear bright in Magellan SAR. "Fresh" appearing craters have bright,

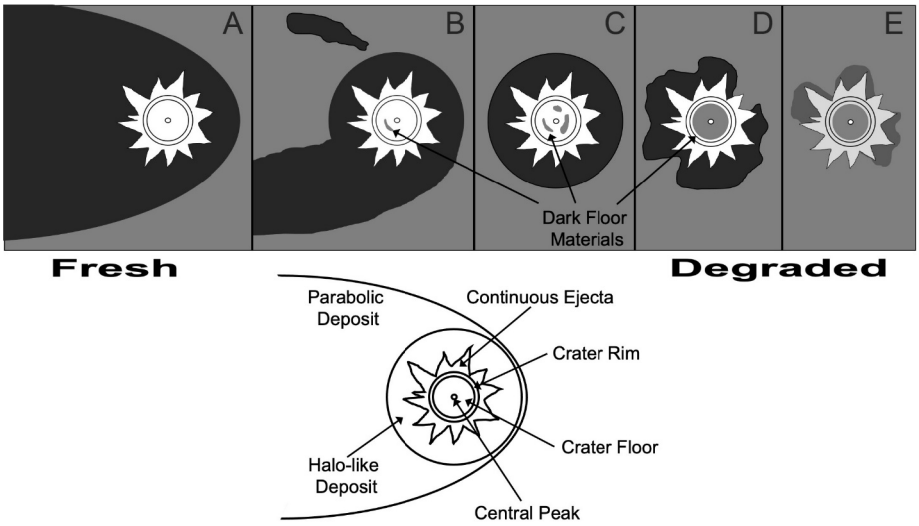

Fig. 4 Model of crater degradation on Venus, from Izenberg et al. (1994). **A**) Crater forms with high backscatter rim, bright floor and continuous ejecta, and low backscatter halo and parabola ejecta deposits with high contrast relative to surrounding plains. **B**-**E**) Progression of removal of parabola and dark halo, while radar-dark deposits form on the crater floor

rough floors, usually flat. While increasing crater size shows a familiar progression from flat floors to central peaks to peak-rings, there are few simple, bowl-shaped craters on Venus due to atmospheric shielding from small impactors. Many plains craters have fluidized ejecta, and/or dark extended ejecta features or halos that can extend several crater radii farther than the continuous ejecta boundary. The youngest fraction of craters have areally extensive parabolic ejecta features, always opening to the west, resulting from the wind-borne movement of ejecta thrown into the atmosphere's global East-West prevailing winds (Campbell et al. 1992). The parabolas are almost universally superposed on all other surface geologic features, indicating that they are both young and ephemeral. The correlation of the parabolas with dark haloes, radar-bright floors, etc., provides the primary evidence that this is the common appearance of craters immediately after formation (keeping in mind differences as a function of crater size), and that differences from this appearance represent post-impact alteration (Herrick and Phillips 1994a; Izenberg et al. 1994).

There are insufficient numbers of craters to use them as local, or even regional age indicators for the surface, but they are time-stratigraphic markers for their immediate surroundings. Craters, once emplaced, are affected by planetary aeolian, tectonic, and volcanic processes, and the degradation process can be used to better understand local and regional geologic activity (Izenberg et al. 1994) (Fig. 4). For example, the absence of parabolas from most craters, and the existence of both partial parabolas and partial halos infer that surface processes remove or homogenize these features over time. This process could be aeolian removal of the fine ejecta that makes the parabolas and halos appear dark, or volcanic burial, or lithification in place. Crater interiors exhibit a range of potential age effects. While some craters may begin with smooth, dark floors or patches on their floors due to impact melt, some appear to be infilled after formation by volcanic deposits. Bright crater ejecta, on the other hand usually appears pristine unless severely modified or clearly buried by volcanic activity. Crater and continuous ejecta modification by tectonic activity can also be seen in rift zones and in the tessera.

Crater aging degradation on Venus appears morphologically controlled by two vectors: absolute age, and regional activity. A simply aging crater, undisturbed by planetary volcanism or tectonism will evolve from a bright crater with a dark parabola, to a partial parabola, to a halo, to a partial halo, to no halo. The bright interior and ejecta may darken through weathering of rougher blocky materials, and the floor may darken due to interior flooding. Volcanic activity may accelerate the apparent aging process. Low level embayment could very quickly bury/destroy a parabola or halo, while leaving the continuous ejecta apparently untouched. Higher levels of volcanic activity could embay small to large portions of continuous ejecta and potentially breach and flood the crater interior. Significant activity can disrupt crater walls, but lower levels of tectonism may be harder to see in continuous ejecta and crater interiors.

The distinction between crater degradation by volcanism versus mechanical and chemical weathering is important for big-picture resurfacing hypotheses. If degradation proceeds by weathering then the progression shown in Fig. 4 at least loosely represents a defined sequence with time so that the state of a crater would indicate its age of emplacement. If, however, volcanic or tectonic resurfacing play a significant role in degrading craters, then the state of an individual crater conveys only its relative position in the stratigraphic column and little information regarding the absolute age of emplacement. Herrick and Rumpf (2011) have argued that the presence of a radar-dark floor in a crater is not due to weathering but nearly exclusively due to post-impact volcanism, suggesting the latter. Their assessment is based on observations from stereo-derived topography that dark-floored craters, as a family, are shallower than bright-floored craters. That craters with parabolic features all have radar-bright floors (Campbell et al. 1992) argues against craters acquiring dark floors during or shortly after formation through some process like triggered volcanism. They observe no aeolian features such as dune fields in dark-floored craters that would indicate substantial sediment filling, but detailed mapping of several of the largest Venusian craters showed abundant evidence of post-impact volcanism modifying most of these craters (Herrick and Rumpf 2011; Herrick and Sharpton 2000, 1996). Herrick and Rumpf (2011) also found that nearly all dark-floored craters had a portion of the dark halo removed, indicating that if dark-floor formation does indicate volcanic filling that it is probably accompanied by partial volcanic embayment.

On Venus there are a number of near-circular albedo patches with diffuse boundaries that often resemble the dark haloes associated with craters, have no topographic signature or apparent vent associated with them, and are superposed on the terrain with no correlation to local geology (Strom et al. 1994). These "splotches" are thought to be airblast features, similar to the Tunguska event on Earth (Turco et al. 1982), caused by the atmospheric pressure wave created by the disintegration and incineration of intermediate sized impactors (asteroids or comets of ~200 m to 3 km diameter depending on composition and velocity) above the surface due to Venus' thick atmosphere. Splotches may be primarily scour features, but there are indications of ejecta-like materials near some. Stereo imaging may indicate some splotches are slight depressions, however the stereo data lacks enough resolution to form any conclusions. That there seem to be few or no splotches of the ~400 cataloged that are modified by later volcanism has been cited as supporting evidence of a surface that is currently geologically stagnant (Strom et al. 1994).

5 Global Modeling of Resurfacing

Models of resurfacing designed to match some of the general observations can provide constraints and insights on the planet's resurfacing history. The primary observations that the

models in this section try to match are statistical measurements of the spatial distribution of craters and the percentage of craters that have experienced post-impact modification. As the discussion below makes clear, changes in our understanding and interpretation of post-impact crater modification have occurred during the time period in which the modeling has been conducted, so that both the nature of the models and the assumed observational constraints have evolved with time. In general terms, the models can be two-dimensional or three-dimensional, with the latter adding a topographic component to how resurfacing occurs.

5.1 Goals of Resurfacing Models

Proposed models for the geologic history of Venus are tested against characteristics of the cratering and stratigraphic record. First, models of resurfacing should produce the correct number of impact craters on Venus and their size-frequency distribution. On other planetary bodies (Mercury, Moon, Mars, etc.), small craters vastly outnumber large ones because larger impactors are rarer. However, the diameters of impact craters on Venus seem to fit a log-normal probability distribution. Testing resurfacing models against this distribution is difficult because volcanism may have less of an effect on the final size-frequency distribution than two factors that are also quite uncertain: the impactor production function and the atmosphere-impactor interactions. Ultimately, models of resurfacing often draw the diameters of modeled craters from the real size-frequency distribution to guarantee that this constraint is satisfied.

Beyond the number of craters, models of resurfacing can attempt to reproduce statistical properties of their locations. Because impacts are stochastic, it would be absurd to seek to match the exact coordinates of every crater. As discussed above, the distribution of impact craters on Venus is nearly indistinguishable from random. When taken with the relatively low number of total craters, there is no statistically reliable assertion of distinct areal provinces based on crater population.

As discussed above, although the global impact crater distribution is sparse, there are indications that crater distribution may not be random with topography (Herrick and Phillips 1994a), geologic units (Hauck et al. 1998), or global stratigraphy-based geologic maps (Ivanov and Head 2011) and buffered crater counts (Kreslavsky et al. 2015). Nearest-neighbor analysis is one method to determine spatial randomness, which has revealed subtle variation in crater densities across the Venusian plains (Hauck et al. 1998) and clustering among volcanically embayed craters (O'Rourke et al. 2014). This approach has an added benefit of analyzing the distance between a crater and its Mth nearest neighbors, not just its closest neighbor. For example, the obviously embayed craters have random-like distances to their nearest neighbors ($M = 1$). However, they are clustered in groups with $M > 3$. The probability of an intercrater distance between a crater in a dataset with N craters and its Mth nearest neighbor is given by the following formula:

$$p(\theta \mid N, M) = \frac{(N-1)!}{2^{N-1}(N-M-1)!(M-1)!} \sin(\theta)[1-\cos\theta]^{M-1}[1+\cos\theta]^{N-M-1}$$

where θ varies between 0° and 180° (i.e., θ is the smallest angle between the two lines that extend from the center of Venus to the craters on the surface) and thus p is normalized to integrate to 1 over this interval. The probabilistic angular distance between points on a sphere can be compared with the angular distance between observed craters using a normalized test

statistic z defined by:

$$z = \frac{\mu_{\text{exp}} - \mu_{\text{obs}}}{\sigma_{\text{exp}}}$$

where μ_{exp} and μ_{obs} are the calculated and observed mean angular distance and σ_{exp} is the standard deviation of the probability distribution function. A smaller population (low N) would have σ_{exp} that is relatively large. A perfectly random spatial distribution will have z values close to 0, whereas a surface distribution with either underclustering or overclustering will result in $z < 0$ or $z > 0$, respectively. This test is more sensitive than chi-squared tests on spherical coordinates or intercrater angles, and consequently can provide a more nuanced understanding of the spatial crater distribution.

Finally, successful models of resurfacing should explain the modification states of impact craters. However, as discussed above the underlying observations are controversial. The initial post-Magellan view was that impact craters on Venus are generally pristine with fewer than 10% of total craters showing obvious embayment (Herrick et al. 1997). Unlike craters overall, those obviously embayed craters are spatially clustered (O'Rourke et al. 2014; Romeo 2013; Strom et al. 1994) which could result from volcanic resurfacing concentrated in the Beta-Atla-Themis (BAT) region (Romeo 2013). It is difficult to reconcile the relatively low number of embayed craters with widespread evidence of volcanism across the surface. Consequently, the overall low occurrence of such craters and their spatial clustering remain key observational constraints on any postulated resurfacing history. However, if post-impact volcanism can flood crater floors through cracks and small breaches in crater rims, 750 dark-floored craters would be reclassified as modified. The proportion of volcanically modified craters would thus increase from ∼10% to ∼80% (Herrick and Rumpf 2011; O'Rourke et al. 2014). Ideally, resurfacing models would consider this ambiguity when determining if a tested resurfacing history is consistent with the observed cratering record on Venus. However, in the extant literature, the number of modified craters is generally considered as a separate question from the spatial randomness of all craters—and no study has fully assessed the spatial distribution of dark-floored craters with respect to topography and geological units.

5.2 Methodology of Resurfacing Models

Modelers face a tradeoff between realism and computational efficiency. Complex models can capture the diversity of volcano-tectonic processes and geologic terrains that is observed on Venus. However, impact cratering is a stochastic process and often volcanism is modeled as a stochastic process, so the outputs of resurfacing models are also stochastic. Statistical comparisons between models and reality require running models repeatedly—thousands of times or more. Specifically, models often use a Monte Carlo approach with a set of random variables that describe how impact craters form and are destroyed over time. Models with more random variables require more model runs (and thus human and computer time) for statistical analyses. Counterintuitively, modelers can thus apply more granular and rigorous statistical tests to resurfacing models that are more abstract and simplified. As in most scientific endeavors, the art of modeling resurfacing on Venus lies in discarding all complexities except those that make a big-picture difference. Monte Carlo models are thus best applied to answering broad questions, such as "was resurfacing catastrophic?"

Resurfacing models must first describe the location, size, and production rate of impact craters. The simplest approach is to assume that impact craters have equal sizes and appear at a constant rate with equal probability at any location on the surface. However, some

additional realism is not too expensive to implement. For example, the size-frequency distribution of modeled craters is often generated from the real distribution (e.g., Romeo and Turcotte 2010) — or with a distribution that is skewed slightly large to account for the likelihood that resurfacing processes preferentially remove smaller craters (e.g., Romeo 2013). Treating cratering on Venus as a Poisson process with a single time constant is reasonable because the surface is relatively young. Studies of planetary bodies with older surfaces such as Mars and Moon are more sensitive to how the impactor production function has changed over geologic time. Finally, Venus is indeed massive enough to homogenize impactor trajectories such that crater locations are isotropic (i.e., with degree-2 variations less than a few percent)—in contrast, the spatial density of impacts on Earth's Moon is highly non-uniform at the ±25% level (e.g., Le Feuvre and Wieczorek 2011).

Global resurfacing models on Venus invoke volcanism as the primary means of removing impact craters from the surface. Two end-member scenarios for volcanism—catastrophic and equilibrium resurfacing—are commonly studied. In models with catastrophic resurfacing, the surface is (mostly) wiped clean by a global episode of intensive volcanism at one time (e.g., Strom et al. 1994). Volcanic activity after catastrophic resurfacing is modeled to occur at a reduced rate (e.g., Romeo 2013) and, often, only at certain locations such as the Beta-Atla-Thema region. In equilibrium models, volcanism occurs at smaller scales at a roughly constant rate over time. Resurfaced patches are modeled as circular areas, which have sizes that are scaled to the frequency of resurfacing and cratering events to reproduce the correct number of craters on the surface of Venus today. For example, if one crater is produced every Myr, then a model where resurfacing events occur every Myr and each cover ∼0.1% of the surface will produce ∼1000 craters in equilibrium and a cratering age of ∼1 Gyr. Tectonic processes can also destroy (or at least obscure) craters, especially in tesserae, but are usually ignored in resurfacing models—or tacitly treated as equivalent to volcanism.

In general, existing craters can be unaffected, modified, or destroyed by resurfacing events. Different models take different approaches to quantifying when each outcome occurs. In perhaps the most basic model, the resurfacing event is described with one number: the radius of the circular region covered by a volcanic flow. In this model, craters are unaffected if they lie fully outside the resurfaced region; they are modified if some portion of the crater is touching the resurfaced area; and they are fully destroyed if they lie within the resurfaced area (e.g., Schaber et al. 1992). This simple model is computationally efficient but imposes an unrealistic assumption that fresh crust will always fully cover existing craters in the area. In reality, crater rims are a non-negligible elevation feature—and it is unrealistic to assume that volcanic flows will always be thick enough to bury them. This shortcoming can be addressed in models by adding an annulus around the resurfaced patch and tagging craters within that annulus as "modified craters" (e.g., Bjonnes et al. 2012). Resurfaced patches modeled this way more closely represent volcanic flows which are thicker near their point of origin, presumably the center of the circular resurfaced patch, and get thinner toward the edges to the point where it is not enough to fully cover existing features. The width of the annulus can be adjusted relative to the radius of the inner portion to simulate different lava viscosities. Preexisting craters would then be marked as "completely erased" if they are in the center portion of the resurfaced patch, "modified" if they fall within the defined annulus, or "unaffected" if they are fully outside the resurfaced area. Finally, another type of Monte Carlo model treats volcanic units as three-dimensional cones (Romeo 2013; Romeo and Turcotte 2010). Geological maps provide the edge angles of these cones (e.g., from ∼0.2–2°) and the frequency-area distributions of the units (e.g., from $>10^6$ km^2 to <20 km^2). In these models, a volcanic unit modifies a crater if the cone is tall enough to cover the crater's rim, using distributions of rim heights and crater diameters derived from bright-floored craters (e.g., Herrick and Sharpton 2000).

Another model of resurfacing was developed in response to the idea that volcanism has modified up to ∼80% of the impact craters on Venus (Herrick and Rumpf 2011; Herrick and Sharpton 2000; Wichman 1999). Like the simplest model, resurfacing patches are circles defined by a single radius. However, in these new models, multiple resurfacing events are required to destroy an impact crater (O'Rourke et al. 2014). Craters that are tagged with fewer than a critical number of resurfacing events are considered modified. If five resurfacing events are required to completely bury crater, then 20% (i.e., 1/5) of the total population will remain pristine in equilibrium. Critically, the horizontal radius of the patch does not affect the final proportion of pristine craters in this type of model. If the average crater has a rim-floor depth of ∼1 km (Herrick and Rumpf 2011), then this ratio of pristine-to-modified craters implies that one resurfacing patch involves extrusive flows that have thicknesses of ∼200 m. In this model, small craters are preferentially erased because they have shallow rim-floor depths. Finally, the radius of the resurfacing patch then controls the spatial clustering of the pristine and modified craters—small patches lead to random-looking distributions.

In the aftermath of the Magellan mission, many scientists claimed that only catastrophic resurfacing was consistent with the cratering record. Immediately after global maps were available, Phillips et al. (1992) showed that either catastrophic or equilibrium models could create a random-looking spatial distribution of all craters. However, others then argued that the ostensibly low fraction of modified impact craters (∼10%) was inconsistent with equilibrium resurfacing. Strawman models were developed that used very small resurfacing patches with proportionally thick annuluses, meaning that volcanic events were almost as likely to modify as destroy craters (Schaber et al. 1992; Strom et al. 1994). Several studies (Bullock et al. 1993; Romeo 2013; Romeo and Turcotte 2010) developed perhaps the most elaborate version of this model—the shapes of volcanic flows and the diameters and rim heights of craters were all drawn from different distributions and modeled in three dimensions. Their catastrophic resurfacing models naturally predicted a low proportion of volcanically modified craters—planet-wide volcanism destroyed rather than modified all extant craters, then volcanic events were concentrated at certain locations (such as the Beta-Atla-Themis region) and occurred at drastically lower rates (e.g., Romeo 2013).

In the last decade or so, equilibrium resurfacing models were refined to show that they can also produce the correct proportion of modified craters. The approach of using a global resurfacing model with variably-sized resurfacing patches and an annular rim wherein craters are modified and not fully destroyed was implemented by Bjonnes et al. (2012). They ran a series of Monte Carlo models testing the effects of resurfacing between 0.01 and 50% of total surface area per resurfacing events, concurrent with impact crater formation throughout Venus' history. Their results show that resurfacing the planet in areas approximately 0.1–1% of total surface area replicates both the seemingly random spatial distribution of craters across the surface as well as the low number of obviously embayed craters. This approach used the more realistic method of incorporating a ring around the resurfacing patch where craters would be embayed rather than destroyed. However, these models randomly selected points for the centers of resurfacing patches, which is inconsistent with observations that some regions on Venus are more geologically active than others. Consequently, the simulated locations of embayed craters were also randomly distributed across the planet. However, nearest-neighbor analysis shows that observed embayed craters are clustered for >3rd nearest-neighbor distances (O'Rourke et al. 2014). Other studies tested equilibrium models with non-uniform spatial distributions and temporal rates of volcanic resurfacing (Romeo 2013; Romeo and Turcotte 2010). Future work could augment these models to allow for even more complex scenarios consistent with new models of Venus's geodynamic evolution (Rolf et al. 2022).

Ultimately, Monte Carlo models that represent either catastrophic or equilibrium resurfacing can reproduce the first-order properties of the cratering record, including the number of impact craters, their size-frequency distribution, their spatial clustering (or lack thereof), and the proportion of craters modified by post-impact volcanism. Claimed inconsistencies between equilibrium models and reality often result from unrealistic assumptions in the models that were made to reduce the parameter space to a manageable size for a single study. For the next generation of Venus exploration, scientists should tie models of cratering and resurfacing to newly available information about the geologic history of the surface—and to increasingly sophisticated simulations of how the deep interior of Venus has evolved over time.

5.3 Resurfacing Models Coupled to Mantle Convection

The techniques outlined in the previous subsections are powerful methods to efficiently map out controls on the surface age distribution and its link to the crater population. However, they do not fully capture the physical processes driving resurfacing, which on Venus are likely a combination of volcanism (lava flows) and tectonism (crustal deformation). Mantle convection is the physical mechanism controlling the thermal and stress state of Venus' crust (Rolf et al. 2022, this collection) and therefore the spatiotemporal evolution of resurfacing. Classically, surface age may be inferred from mantle flow using half-space cooling (see Turcotte and Schubert 2017) in which case surface age is a simple function of heat flux (e.g., Labrosse and Jaupart 2007). However, this approach has several limitations and importantly assumes the lithosphere to be mobile (i.e., to move with rates comparable to that of mantle flow), which is unlikely the case for present Venus. Instead, tracer particles may be used to either track when a respective material patch last melted and rose to the surface (e.g., Noack et al. 2012) or how long a tracer resides in a layer close to the surface (Karlsson et al. 2020; Rolf et al. 2018; Uppalapati et al. 2020). The latter approach captures both tectonic and volcanic resurfacing self-consistently—but has limitations, for instance, regarding the thickness of the layer defined as 'surface'. In addition, existing planetary-scale models typically only track magma ascent to the surface, but not the subsequent lateral lava flow across Venus' surface. The modification of craters by the resurfacing processes is also beyond the capability of current models.

Nevertheless, such physics-based approaches have proven useful to tie resurfacing to the state of the interior. Although sophisticated simulations of mantle convection are too intensive to run tens of thousands of times in a Monte Carlo framework, they can provide guidance about big-picture issues such as the age of the surface and whether resurfacing is catastrophic. For example, a cooler mantle may yield a larger mean surface age, because lower temperatures lead to less mantle melting and thus suppress volcanic resurfacing rates. Catastrophic resurfacing episodes can cool the mantle more efficiently and may promote an older surface, on average. However, this strongly depends also on the eruption efficiency of magma as intrusive magmatism will less efficiently destroy surface craters than extrusive lava flows. Only recently have mantle convection models become capable of realizing low eruption efficiencies (e.g., Lourenço et al. 2020) which are more likely relevant for Venus in its more mature stages of evolution.

In the episodic scenario, surface age also strongly depends on the style of the resurfacing episode. In the classic form, an episode resets surface age globally leading to a uniform surface as inferred for Venus. Extinct (or very limited) volcanism after overturn cessation then allows for uniformly increasing mean age without degenerating the age uniformity. However, models of Venus' mantle convection indicate a more complex process: Lithospheric

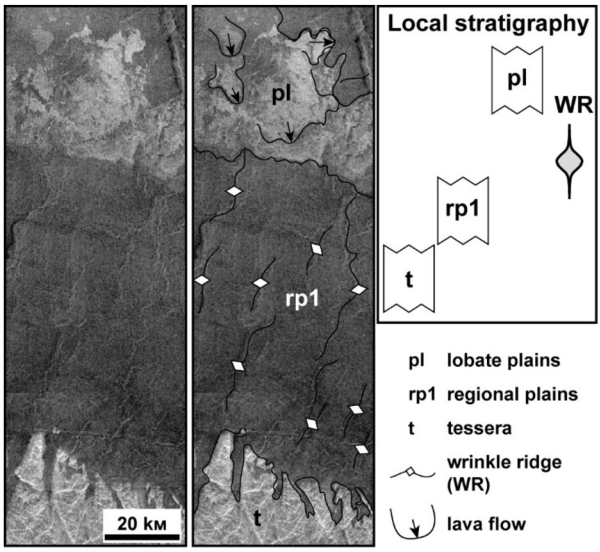

Fig. 5 Typical age relationships among tessera (t), the lower unit of regional plains (rp1) and lobate plains (pl). These relationships are repeated in each region of Venus where these units are observed

mobilization during the episode may not be global (Gillmann and Tackley 2014; Noack et al. 2012; Romeo and Turcotte 2008) and portions of the surface may not be recycled (e.g., Karlsson et al. 2020; Uppalapati et al. 2020; Weller and Kiefer 2020). Even if global, resurfacing does not occur simultaneously across the surface, but propagates during ~100–200 Myr or more depending on the duration of such events (e.g., Armann and Tackley 2012; King 2018; Rolf et al. 2018). As a consequence, substantial variations in surface age exist during essentially any time. Important steps of future work are thus to identify whether this variability in surface age is due to model limitations or whether it applies to Venus, perhaps on scales that are poorly captured by the sparse density of craters on Venus.

6 Resurfacing Constraints from the Geologic Record

6.1 The Case for a Global Stratigraphic Sequence

The idea of a global stratigraphy for Venus is based on two key interpretations made during a photogeological analysis of 36 randomly selected regions (Basilevsky and Head 1995, 1994): (1) in all cases, sets of morphologically distinct units that make up the surface were relatively small and repetitive, (2) all these units show similar relationships of relative ages and, thus, form similar stratigraphic sequences. Support for the idea of a global stratigraphy came from the results of the USGS program of geological mapping of Venus. These mapping efforts in different regions of Venus have indicated existence of a general progression of units from the oldest strongly tectonized terrain, such as tessera, through a ubiquitous unit of regional plains at middle stratigraphic level, to the youngest plains characterized by prominent internal flow-like features (Fig. 5).

Basilevsky and Head (1995, 1994) have summarized their observations in the form of a hypothesis that the geological record of Venus is made up of globally correlative units and that the accessible geologic history of the planet consists of a series of specific episodes when different volcanic and/or tectonic processes dominated (Basilevsky and Head III 1998;

Herrick 1994). This hypothesis is broadly consistent with the lack of evidence of plate tectonics during the observable part of the Venus' history and suggests a possible alternative mechanism of internal heat loss, primarily conduction through a static lithosphere over a convecting mantle (e.g., Solomon et al. 1991; Solomon and Head 1982). To test the applicability of the observations made in isolated areas (Basilevsky and Head 2000, 1995, 1994), geological mapping in sizable and, most important, contiguous areas was required. Ivanov and Head (2001b) thus attempted such a test by compiling a geologic map consisting of a geotraverse centered at 30°N that extended completely around the Venus globe and connects several isolated regions. The mapping results in the geotraverse revealed that regional plains with uniform morphology can be traced continuously for thousands of kilometers and link remote regions. This extensive and pervasive unit everywhere in the geotraverse embays most of heavily tectonized units (e.g., tessera, ridge belts, and groove belts) and is superposed by flows of lobate plains (Fig. 5). The observations made during mapping of the geotraverse and in several USGS quadrangles (Ivanov et al. 2010; Ivanov and Head 2001a, 2008, 2006, 2005, 2004) have suggested that only a small number of units with clearly different morphology make up the majority of the surface of Venus. These findings allowed a compilation of a global geological map of Venus at 1:10,000,000 scale that portrays the distribution of the defined units/terrains in space and time (Ivanov and Head 2011). The global map has shown that the defined units (1) clearly describe the variety of morphologies at the global scale, and that (2) they form a generalized sequence that consist of three major (composite) units: (1) the older tessera, labeled "t" (and the other heavily tectonized terrains), (2) mildly deformed regional plains, labeled "rp" (and the other units of the plains volcanism), in the middle of the generalized sequence, and (3) mostly non-tectonized lobate plains, labeled "pl", at the top of the sequence (Fig. 5).

The findings made during compilation of the global map suggest that the preserved geologic record of Venus (the last < ∼1 Ga) is mostly consistent with a mechanism of the internal heat loss that is radically different from the global plate tectonics mode of heat loss that has characterized Earth through much of its history (Rolf et al. 2022), and that may even have had an episodic character (Parmentier and Hess 1992; Turcotte 1993).

The characteristic age relationships of units shown in the global map suggest that the accessible part of the geologic history of Venus consists of three major episodes, each with a specific style of resurfacing (Fig. 6) (Ivanov and Head 2015): (1) A global tectonic regime, when tectonic resurfacing dominated. Exposed occurrences of units of this regime comprise ∼20% of the surface of Venus. (2) A global volcanic regime, when volcanism was the most important process and resurfaced ∼60% of the surface of Venus. (3) A network rifting-volcanism regime, when both tectonic and volcanic activity were about equally important. During this regime, ∼16% of the surface of Venus was modified.

The global tectonic regime is defined by units labeled t (tessera), pdl (densely lineated plains), pr/RB (ridged plains/ridge belts) and gb (groove belts). Ridges of tesserae and ridge belts suggest that compressional forces dominated during the earlier phases of the global tectonic regime. They were responsible for the formation of the bulk of the tesserae over the sites of mantle downwelling. Ridge belts are due to limited horizontal displacement and warping/buckling of crustal materials at the periphery of the major convective cells where downwelling takes place (Gilmore and Head 2018, 2000). Groove belts characterize the later phase of the global tectonic regime. The scales of the features of the global tectonic regime suggest that they reflect the ancient pattern of mantle convection.

During the global volcanic regime, vast volcanic plains (shield and regional plains, the lower and upper units) were emplaced. These plains have different morphologies that indicate different volcanic styles: (1) eruptions from small, abundant, and broadly distributed

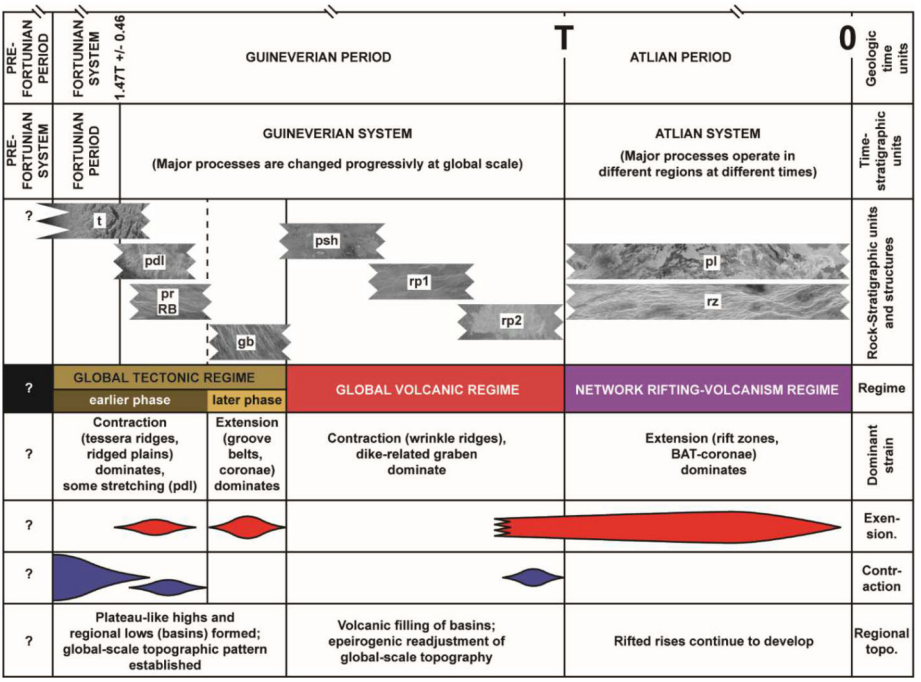

Fig. 6 Three major regimes of resurfacing (see text for discussion). Modified from Ivanov and Head (2015)

sources (psh, shield plains), (2) voluminous eruptions from near globally distributed sources (rp1, lower ridged plains unit), and (3) eruptions that have been concentrated within specific regions and around some large volcanic centers. The major tectonic structures of the global volcanic regime are wrinkle ridges and graben swarms radiating from distinct volcano-tectonic centers (Bilotti and Suppe 1999; Ernst et al. 2003, 2001, 1995; Sandwell et al. 1997). Both types of structures deform the surfaces of the vast plains but are not related directly to specific patterns of mantle circulation.

Approximately equally abundant volcanic and tectonic processes of the formation of lobate plains and rift zones characterize the youngest network rifting-volcanism regime. Rift zones that constitute its tectonic component are very prominent but their total area is about four times smaller than the exposed area of terrains of the global tectonic regime. This means that the tectonic resurfacing diminished with time and evolved from the broadly distributed deformation during the earlier global tectonic regime to the highly concentrated deformation during the later network rifting-volcanism regime. The numerous flows of lobate plains suggest multiple episodes of volcanic activity during the network rifting-volcanism regime. The areal distribution of lobate plains implies that their sources were discrete and that they formed in different areas at different times. The apparently prolonged and broadly synchronous formation of lobate plains and rift zones are fundamentals of the nondirectional model of the geologic history of Venus (Guest and Stofan 1999). This model adequately describes the later stages of the history, whereas the alternative, evolutionary, model (Basilevsky and Head III 1998; Ivanov and Head 2011) embraces the entire assessable portion of the geologic history of Venus.

Impact craters with the surrounding dark mantling materials (parabolas/haloes) are considered as the youngest impact structures on Venus (Campbell et al. 1992). Indeed, the rel-

ative abundance of such craters suggests that craters with prominent dark parabolas may have been formed during the last 0.1-0.15T (where "T" is the mean model age of the surface of Venus) and lifetime of craters without parabolas but with distinct haloes is about 0.3T (Basilevsky and Head 2002). These estimates of the dark parabolas/haoles lifetime suggest that the youngest lobate plains of the network rifting-volcanism regime at Beta Regio are younger than about 0.5T and those at Atla Regio may be as young as about 0.1-0.15T (Basilevsky and Head 2002).

6.2 The Case for a "Non-directional" Geologic History

6.2.1 Material Units and Tectonic Structures

Stratigraphic sequences are normally defined on the basis of lithological units (e.g. through sedimentary logging), although biostratigraphy is of course commonly used on Earth because of the abundance of fossils in the Phanerozoic. Mappable units are defined on the basis of common features, such as the 'grey chalk' in distinction to the 'white chalk'. Gaps in succession (unconformities) often indicate episodes of tectonic uplift (orogenies), but these are of course not recorded in the stratigraphic sequence: for example, the Carboniferous Coal Measures do not grade into the Variscan orogeny and then into the Mercia Mudstone, but instead the Mercia Mudstone directly and unconformably overlies the Coal Measures. Geological structures do not feature in the sequence for two reasons: in this example, Variscan structures overprint all older material units, regardless of their age, and so do not correspond with any particular material unit; and additionally, these structures can be reactivated and so appear younger than they really are.

Distinguishing material units separately from structural relationships (Hansen 2000) is therefore helpful for inferring the sequence of tectonic events from kinematic analysis. Structural relationships can often be counter-intuitive, e.g. a straight fracture is more likely the oldest structure, not the youngest. Younger fractures sense the presence of older breaks (because they act as free surfaces) and deviate towards or away from them and, as noted, suitably oriented fractures may be reactivated by later events, sometimes in reverse (i.e. inversion). This can make the extremely fractured surface of Venus difficult to decipher.

6.2.2 Mappable Radar Units

One of the major problems for lithostratigraphic mapping on Venus is that radar is quite insensitive to lithological units, except in the rare instance of a marked difference in relative permittivity (usually in relation to iron content). Instead, radar is sensitive to surface roughness on the scale of the radar wavelength (particularly near the Rayleigh criterion), small-scale slopes, and other surface textures. An example from Earth nicely illustrates this problem (Fig. 7): contrast changes in the radar image only sometimes correlate with geological boundaries, while particularly significant features, such as the Mid-Atlantic ridge, and the edge of the Vatnajökull ice cap, are almost invisible in the radar image. Even fresh lava flows can prove difficult to map, apparently disappearing in the radar image where their flow becomes laminar, and reappearing where a'a or pahoehoe-textured areas. A more serious problem is that very different lithostratigraphic units can appear identical in a radar images: 100 Ma old Upper Greensand Sandstones look very similar to 800 Ma old Torridon Sandstones, but very different to the almost coeval Gault Clay deposited farther offshore. Worse still, a thin sedimentary veneer is sufficient to completely erase contacts between different units. The reason that large parts of Fig. 7 appear similar is that they are covered by alluvial sediments.

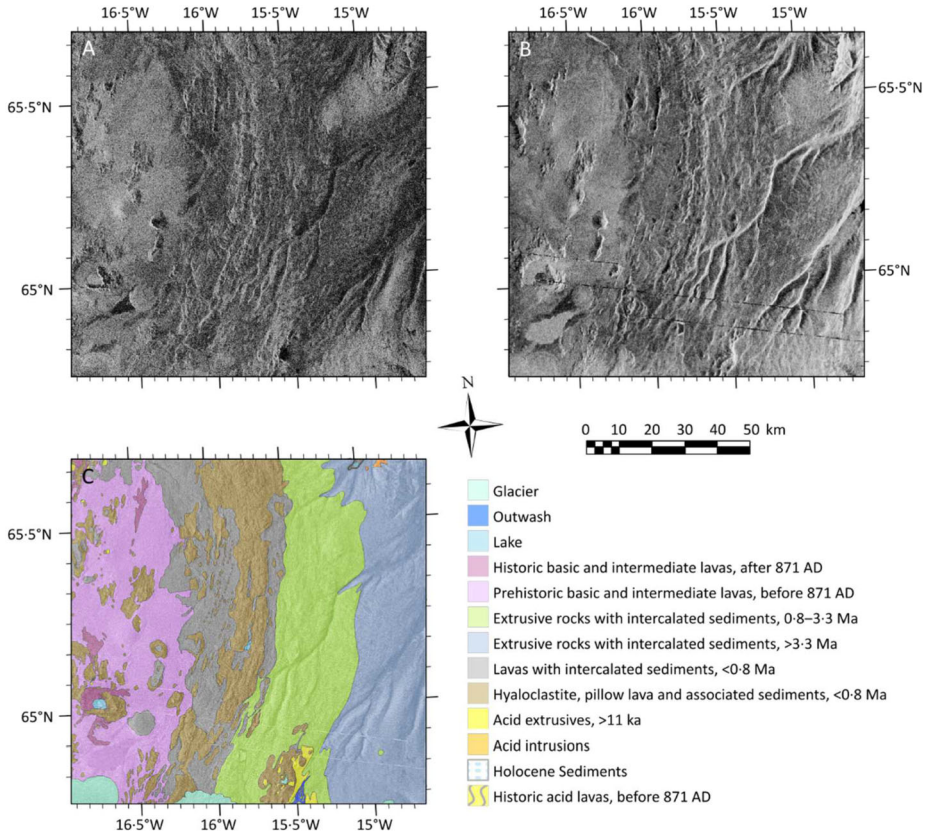

Fig. 7 Simulated Magellan radar images and geological map of the Vatnajökull National Park, Iceland, illustrating the difficulty in identifying geological boundaries from radar imagery. Oskjuvatn volcano is in the lower left (65·0°N, 16·8°W) with the Holuhraun eruption that occurred between the image acquisitions to the south. [A] Sentinel-1A left-look (descending) image acquired on 24 September 2016, degraded to simulate Magellan Cycle 1 image. [B] Sentinel-1A right-look (ascending) image acquired 22 December 2014, degraded to simulate Magellan Cycle 2 image. [C] Shaded relief geological map based on data from The Icelandic Institute of Natural History showing that neither the boundary between the European and North American plates (approximately N-S through the centre of the image) nor the Vatnajökull ice cap (bottom) are obvious in the radar images, despite their geological significance. Note that the growth of the Holuhraun lava flows from 70 to 85 km^2 (and in volume from 1·0 to 1·6 km^3) in the nine months between radar images is not apparent given the significant changes in appearance caused by the changes in viewing geometry

Nearly a third of the Venus surface comprises indistinct plains; not featureless, but lacking traceable boundaries or features, most likely because these plains are covered by a veneer of sediments of the type observed in the Venera lander images (see Carter et al. 2023, this collection). A veneer only tens of centimetres thick is sufficient to obscure boundaries and break down global stratigraphic relationships.

6.2.3 Radiometric and Spatial Resolution

As the average roughness of a surface declines through the Rayleigh criterion, which is close to 2 cm for the Magellan radar, the backscatter brightness changes by ∼12 dB from bright (an average roughness of 4 cm for Magellan, corresponding to a pebbly surface) to dark (at

0.5 cm, typical of gravel). Such a change can occur over a relatively short distance, perhaps only 100 m on debris slopes and fans, which might be just one or two pixels at Magellan resolution (110 m along track and between 101 and 250 m across track) and therefore can appear as an abrupt change that may be misinterpreted as a geological boundary or contact.

Lithostratigraphy from radar images is therefore fraught with difficulty and should be avoided, except in circumstances where different lithologies can be identified with confidence (clearly defined lava flows, for example). More usually, mapping should be geomorphic, to which radar is exquisitely sensitive, which typically means a focus on geological structures and sedimentary processes.

In short, there are two key assumptions that are linked to the global stratigraphic sequence interpretation and its timing based on crater degradation. First, surface geologic units that have been deposited at different times must always be separable, and within a geologic unit there cannot be boundaries that can be confused with stratigraphic boundaries. Second, using crater degradation/alteration to determine the relative timing of this sequence assumes a spatially uniform timing of the degradation process (e.g., parabolas associated with craters are always removed by weathering at a uniform rate). If these assumptions are widely violated, then it becomes impossible to distinguish between a lunar-like directional model (Ivanov and Head 2011) and an Earth-like nondirectional model of Venus stratigraphy using Magellan radar data alone. A key point of (Hansen 2000) was an illustration of how a variety of completely different geologic histories could result in a final landscape that appears identical in Magellan-resolution SAR images.

7 Evidence for Young and Active Volcanism

In this section we discuss three general approaches to searching for evidence of recent or ongoing volcanism. In the first two sections we discuss properties of imaging at radar and infrared wavelengths that may be indicative of young, chemically unweathered surfaces. We then explore radar signatures indicative of mechanical weathering and/or sediments that have been used to infer the presence of young volcanic deposits. Finally, active volcanism can potentially be observed through observation of a thermal signature or changes between images taken at different times.

7.1 Radar Emissivity

The Magellan mission observed the thermal emission of the surface at 12.6 cm wavelength, which together with surface temperature inferred from descent probes and Magellan altimetry provides radiothermal emissivity with a resolution of 20 to 80 km, depending on latitude (Pettengill et al. 1992). Radiothermal emissivity is affected by the dielectric permittivity of the surface, shape of the surface at the scales of the radar wavelength, and emission angle, the latter of which varied with latitude due to the orbit of Magellan. The most striking feature of this map is a steep reduction of the radiothermal emissivity to unexpectedly low values above a critical elevation, which varies from location to location to between 6053.6 to 6056.4 km radius (Pettengill et al. 1992).

The cause of the low emissivity and the complementary high radar reflectivity at high elevations is still a matter of debate (Brackett et al. 1995; Fegley Jr. 1997; Fegley Jr. et al. 1997; Klose et al. 1992; Pettengill et al. 1992; Shepard et al. 1994; Wood 1997), but in general terms the elevation boundary is interpreted to be a temperature boundary across which elements with a high dielectric constant become stable. The temperature of the surface

of Venus likely only has small lateral gradients due to the efficient redistribution of heat by convection in combination with small solar heating and radiative cooling rates (Stone 1975), and the temperature is thought to decrease vertically by a little less than 8° C/km (Seiff et al. 1985). Using the highest resolved temperature profile of the lowest 10 km by the VeGa 2 probe (Team and Seiff 1987), this critical elevation corresponds to temperatures between 720 and 700 K (Brossier et al. 2020).

As with formation of a weathering rind on Earth, it is hypothesized that the high-dielectric surface minerals form over a geologically significant time period, perhaps up to millions of years (Robinson and Wood 1993; Wood 1997). Places where there is a significant departure from an expected elevation "snow line" of high reflectivity / low emissivity can be interpreted as where something has occurred recently enough that the normal weathering process has not had time to operate. Robinson and Wood (1993) identified volcanic features and flows with anomalous emissivities and interpreted them to relatively recent volcanism, and speculated that Maat Mons has undergone the most recent episode of volcanic activity. More recent work with Magellan emissivity data (Brossier et al. 2022, 2021, 2020) has affirmed this interpretation, indicated additional sites of young volcanism on larger volcanoes, and suggested recent volcanic activity in Ganis Chasma.

7.2 Near Infrared Emissivity

The Venus atmosphere features atmospheric windows in the near infrared, where surface thermal emission can be observed on the night-side. The VIRTIS instrument on the Venus Express mission (Piccioni et al. 2007) observed this radiance at 1020 nm wavelength, and detected locations that feature thermal emission that was up to 15% higher than other locations with the same surface elevation (Erard et al. 2009; Mueller et al. 2008). VIRTIS observed thermal emission in two additional surface windows at 1100 nm and 1180 nm but in these bands the radiance anomalies are not significant even at the most frequently observed area in Themis Regio (Kappel et al. 2016; Mueller et al. 2020), likely due to higher atmospheric opacity decreasing the surface signal.

The areas with increased emission at 1020 nm are interpreted as higher emissivity because 1) the Venus atmosphere is efficient at redistributing heat via convection, allowing only for small lateral temperature gradients in the lower atmosphere (Seiff et al. 1985; Stone 1975), 2) the anomalies persist over the 2 years of observation and 3) the anomalies are correlated with lava flow features at the flanks of volcanic centers such as Quetzalpetlatl Corona (Helbert et al. 2008), and Themis and Imdr Regios (Mueller et al. 2008).

Smrekar et al. (2010) argue that chemical weathering reduces the emissivity of basaltic surfaces over time by breakdown of high emissivity mafic minerals to lower emissivity minerals such as quartz, anhydrite, and very fine hematite. The high emissivity anomalies correlate with locations where gravity and topography data indicate an active mantle plume (Ivanov and Head 2010; Smrekar 1994; Stofan et al. 2016). Smrekar et al. (2010) therefore conclude that these high emissivity anomalies associated with stratigraphically young lava flows represent unweathered and thus relatively recently resurfaced areas.

It is currently not clear what average rate of resurfacing this interpretation implies. An alternative explanation to chemical weathering for a reduction of emissivity with time, could be the deposition of micrometer thin layers of fines produced by impacts. The timescales at which chemical weathering reduces emissivity has been estimated at widely diverging values, from hours in not entirely realistic laboratory conditions (Filiberto et al. 2020) to 0.5 Ma from theoretical calculations of reaction kinetics (Dyar et al. 2021). A weathering timescale of hours is close to the cooling timescale of lava flow, thus if the estimates of Filiberto et al.

2020 are correct, the radiance anomalies would correspond to a mix of temperature and emissivity contributions.

Atmospheric blurring reduces the spatial resolution to 90 to 100 km (Basilevsky et al. 2012; Hashimoto and Imamura 2001). It is possible to identify large flow fields that could be responsible for the high emissivity (D'Incecco et al. 2017), but with the current data quality it is not possible to state whether the emissivity anomaly is due to a few flow lobes with high thermal emission or a moderate increase of emissivity over the whole flow field. An unweathered area needs to be on the order of 10,000 km^2 for an unambiguous estimate of its emissivity difference.

The observed radiance anomaly of up to 15% does not directly translate into an emissivity difference due to the non-linear relation of top-of-atmosphere radiance and surface emissivity (Hashimoto and Sugita 2003). At high absolute emissivity, a relative anomaly in radiance indicates a higher relative change in emissivity, e.g. a 1% change in emissivity results only in a 0.3% change in observable radiance (Dyar et al. 2020). Uncertainties in the absolute emissivity, i.e. the global average emissivity, are large due to uncertainties of atmospheric opacity and surface temperature (Kappel et al. 2015). In-situ spectrophotometry from the Venera 9 and 10 landers (Ekonomov et al. 1980) indicates an emissivity of ∼0.85 to 0.9 at ∼900 nm, consistent with unweathered basalt at Venus temperatures (Helbert et al. 2021). This means that either (1) these locations are unweathered, or (2) there is a steep decline in emissivity from 900 nm to 1020 nm in the weathered basalt, or (3) some of the radiance anomalies reported in Helbert et al. (2008), Mueller et al. (2008) are in fact not due to an emissivity anomaly.

Thus, overall it is difficult to use the thermal emission data for dating surfaces. Some progress seems possible in the near future. If DAVINCI happens to descend at a location with a basaltic inter-tessera plains, observations from below the bulk of the atmosphere might constrain the absolute reflectance/emissivity of weathered basalt at 1020 nm. An analysis of the Venera 13 and 14 spectrophotometer data could also provide more insights, since the spectral range extends to 1200 nm. An experimental confirmation of the long timescale of weathering proposed by Dyar et al. (2021) is difficult, as is the production of analog samples weathered under accurate Venus conditions for such timescales.

A way forward could also be an independent estimate of the rate of volcanism specific to the locations with increased emissivity. The volcanic activity of mantle hotspots on Earth, an apparently close analog to the Venus hotspots, is routinely monitored by satellites (Wright et al. 2015). Hotspot eruptions are relatively frequent, and a significant fraction of Earth's eruptions would be detectable through the clouds of Venus (Mueller et al. 2017). If sufficient IR data is gathered by instruments on the coming Venus orbiter missions to detect a robust statistic of active volcanic eruptions, this would allow us to constrain the rate of emissivity decrease with time. The observation of a plains resurfacing event appears unlikely, but the rate of emissivity fading with time constrained from hotspot activity would allow us to date plains with increased emissivity, if any are found. A fading timescale of 0.5 Ma and a resurfacing rate of 1 km^2/yr indicate that some not yet fully weathered plains would exist and be detectable, if plains resurfacing is ongoing in patches with at least 100 km diameter.

Bondarenko et al. (2010) interpret radiothermal data at Bereghynia Planitia as result of emplacement of a 200,000 km^2 lava area within decades preceding the Magellan mission. This area was not observed by VIRTIS but could be by future missions.

7.3 General Radar Properties

Radar backscatter is affected by the cm-scale morphology of the surface. It is possible that this morphology changes over time, and if so this might be used to date surfaces. Camp-

bell and Campbell (1992) studied the incidence angle and polarization dependence of radar backscatter in comparison to Earth analogs and concluded that the surface roughness of most flows is comparable in roughness to pahoehoe flows on Earth, characterized by a crust that has not been disrupted during the emplacement of the flow. Campbell and Campbell (1992) also note that the large lava flows on Venus imply high eruption rates which favor the formation of aa flows, where the flow surface is continuously disrupted during emplacement and is thus covered in rubble. Bruno et al. (1992) studied the outline of Venusian flows and find that their fractal dimensions are more indicative of aa flow. Kratter et al. (2007) studied the huge, radar bright flow field (600,000 km^2) associated with Quetzalpetlatl Corona on the south flank of Lada Terra and found that its radar properties are mostly consistent with pahoehoe flow roughness. Stofan et al. (2001) studied the flow fields of some volcanoes in Magellan radar images and found some evidence of crust disruption during flow emplacement. Some flows have bright margins, interpreted to be blocky levee material; on Earth such flows form when a flow pushes disrupted crust material in front of it.

One possible explanation for the dearth of aa-like surface roughnesses (Campbell and Campbell 1992) is that erosion from physical or chemical weathering reduces the surface roughness over time. Campbell et al. (2017) noted that the bright diffuse deposits they interpret as cm-sized pyroclasts appear to be absent from everywhere except the latest part of the stratigraphic column, and they consider rapid weathering as a possibility. If cm-sized clasts rapidly disappear from the radar signal, the decimeter-sized rubble of a flow with aa texture should disappear soon after.

Potential mechanisms for reducing cm- and decimeter-scale roughness are wind erosion and chemical weathering. Zolotov and Volkov (1992) discuss aspects of chemical weathering on Venus. An alternative explanation could be the reduction of surface roughness by airfall deposits. Basilevsky et al. (2004) suggest that the surfaces in the Venera panoramas that had been interpreted as pahoehoe lava flow (Garvin et al. 1984) are actually lithified aeolian sediments from impact ejecta.

Whatever processes produce a modification of surface roughness over time, it is clear that only surfaces that have some initial roughness are significantly affected by it. To use surface roughness as an age proxy would require one to have a measure of the initial roughness. Future missions with highly resolved images and topography data might be useful in identifying features that could be indicative of flow texture, such as blocky levees for aa flows (Stofan et al. 2001) or inflation features on pahoehoe flows (Voigt et al. 2021). For mostly featureless plains, this approach does not seem promising.

7.4 Radar Properties of Potential Young Pyroclastics

Radar-bright diffuse deposits near the summit regions of some coronae have been proposed to be young pyroclastics, and possible evidence of a renewed epoch of mantle volcanism that taps into deeper volatiles (Campbell et al. 2017). The deposits have radar properties associated with rough terrain, including high backscatter and an increased circular polarization ratio in Arecibo Observatory images compared to the surrounding plains. (Circular polarization ratio is a measure of the same sense circular polarization transmitted to the opposite sense polarization; rougher surfaces generate higher CPR values.). The radar-bright features also have emissivity values that are similar to the plains or only slightly lower, so there is no evidence that they are a high-dielectric coating as is seen in other regions of Venus (Campbell et al. 2017).

The deposits are semi-transparent in places, especially near the edges where it is often possible to detect stratigraphically lower features, such as fractures and lava flows. There

is rarely any evidence that the bright deposits are embayed by subsequent flows, and they only appear to have been altered through aeolian processes. There is also little evidence for similar deposits interleaved with other flows. Taken together, these observations suggest that these bright regions are rough mantling pyroclastic flow deposits that are at the top of the stratigraphic column (Campbell et al. 2017). Modeling suggests that the deposits could have been formed through column collapse or perhaps long duration fire-fountaining, with thicknesses ranging from meters to tens-of-meters (Ganesh et al. 2021). Their presence indicates that significant volatiles (CO_2, H_2O) must have been present (Airey et al. 2015), and such volatile-rich eruptions are more typical in the early stages of volcanic eruptions (Campbell et al. 2017). These radar-bright deposits may therefore be evidence of renewed activity in these regions, and a good location to search for ongoing volcanic activity.

7.5 Efforts at Detection of Active Eruptions

Detection of active eruptions is here understood to mean all methods that can generate evidence that an eruption took place at a certain location within a short, well constrained timeframe. One such detection has been made using Magellan data, where Herrick and Hensley (2023) found a volcanic vent near the summit of Maat Mons that changed in shape during the Magellan mission. Because the Magellan mission changed viewing geometry with each imaging cycle, and the resolution of the SAR imaging is 100-200 m, only multi-kilometer shape changes in objects can be confidently identified with Magellan data. Future missions, with higher resolution SAR imaging at a consistent viewing geometry, will be much more capable of searching for changes during their missions, and they will be able to look backward for changes since Magellan. Detection of volcanic gas plumes is treated in Wilson et al. (2023, this collection).

Venus surface thermal emission at radar wavelength has been observed by several spacecraft, most importantly the Pioneer Venus and Magellan orbiters. Radar wavelengths are far from the peak of Venus surface thermal emission at 4 μm wavelength temperatures and are not very sensitive to temperature; however, they have the advantage that lava meters below the surface, where the cooling rate is much lower, also contributes to the observable signal. Bondarenko et al. (2010) investigated the Magellan orbiter radiothermal emission (Pettengill et al. 1992) and found that a $\sim 10^5$ km^2 large lava flow unit in Bereghinia Planitia at 28°E 39°N shows an up to 85 K higher than expected brightness temperatures and interpret this as consistent with lava emplaced within the last few decades. Lorenz et al. (2016) argue that this result is ambiguous since it could be explained by a surface emissivity that is different from that derived by Bondarenko et al. (2010) from radar backscatter under assumption of a smooth lava surface. Lorenz et al. (2016) furthermore point out that such a large eruption would be a very unusual event. Assuming that this is not an unusual event, i.e. a statistical expectation of an area of 10^5 km^2 emplaced within the last 100 years, corresponds to a resurfacing rate of 10^3 km^2 / yr, three orders of magnitude larger than the 1 km^2/yr estimated by Phillips et al. (1992) for resurfacing in equilibrium with cratering. Nevertheless, Lorenz et al. (2016) argue that future observations with radiometry with higher spatial resolution than Magellan, ideally accompanied by radar polarimetry to better understand surface roughness and emissivity, would have a good chance of detecting excess thermal emission from a volcano with an activity similar to Mount Etna. However, MacKenzie and Lorenz (2020) studied the radiometry dataset of the Earth observing Soil Moisture Active Passive (SMAP) instrument and found that the detected thermal emission of known active eruptions was lower than expected.

Thermal emission from the surface of Venus can also be detected in near infrared wavelength between 700 and 1200 nm wavelength (Carlson et al. 1991; Wood et al. 2022). The

atmosphere is also mostly transparent in the visible range and therefore an incandescent lava flow (>800 K) could also be detected in this range even if there is otherwise no detectable surface thermal emission. The detection capability in these visible to near-infrared wavelengths is limited by the spatial resolution of ∼100 km imposed by scattering in the permanent cloud layer (Basilevsky et al. 2012; Hashimoto and Imamura 2001; Shalygin et al. 2012). This means that the signature of a lava flow small compared to a 100 km diameter, i.e. the vast majority of lava flows, would appear diffused so that its area cannot be resolved and the maximum of thermal emission is close to proportional to the total thermal emission over the flow. The near infrared thermal emission of an active lava flow is dominated by surfaces close to the eruption temperature, which even on Venus cool to temperatures near ambient on a timescale of hours to a day. Based on this fact it is often assumed in Earth volcano monitoring that the total of the surface thermal emission is proportional to the areal rate at which uncooled lava is exposed, which itself can be assumed to be proportional to the lava effusion rate (Harris et al. 1997; Wright et al. 2001).

Several instruments on Venus Orbiters had capabilities that were estimated to be able to detect eruptions that are not completely outside of the range of historically observed eruptions: the Venus Monitoring Camera (VMC) on Venus Express (Shalygin et al. 2012), the Visible and Infrared Thermal Imaging Spectrometer (VIRTIS) on Venus Express (Mueller et al. 2017), and the IR1 camera on Akatsuki (Iwagami et al. 2011). No detections of eruptions were reported for the VIRTIS and IR1 data, but Shalygin et al. (2015) interpret several VMC images as evidence for active lava flows near Ganis Chasma (18°N, 189°E), south of Ganiki Planitia. This interpretation is based on higher brightness temperature than expected for the respective elevation appearing tied to fixed locations for a duration of a few days. Each of the brightness temperature anomalies have dimensions larger than 100 km, thus if volcanic activity is responsible then it must be distributed over at least 100 km of distance. Three of the four anomalies occur within the same 48 hour timespan along a $\sim 10^3$ km long stretch of the rift. Shalygin et al. (2015) mention that image quality was a limiting factor for detection and that the instrument was able to acquire relatively good data on only 37 days. This suggests that tens of similar anomalies could have been detected with consistently good imaging and the same coverage over a duration of a year. Assuming that the > 100 km long anomalies are caused by 100 km^2 of erupted lava surface, this would indicate a resurfacing rate of $>10^3$ km^2/yr (in the area observed by VMC).

Mueller et al. (2017) unsuccessfully searched the VIRTIS dataset for eruptions. The dataset comprises imaging covering an area equal to six times Venus surface on separate days, limited to the southern hemisphere. The VIRTIS images which would have been able to detect brightness temperature anomalies the same magnitude as those observed by VMC at Ganis Chasma in the northern hemisphere. Assuming eruption effusion rate and duration statistics based on hotspot volcanism on Earth, Mueller et al. (2017) estimate that only at a rate of volcanism > 300 km^3/yr there would have been a high likelihood of an eruption visible. This constraint is weak to the point of uselessness, mostly because only the eruptions with the highest historically observed effusion rates ($\sim 10^3$ m^3/s) would have been detected (Fig. 8). The VIRTIS detection capability was mostly limited by the high instrumental noise, which is proportional to the effusion rate that is reliably detectable. The VIRTIS signal to noise ratio was ∼15; a 20-fold improvement to 300 is planned with the near-infrared cameras for the VERITAS and EnVision missions. This would allow the detection of flows with 50 m^3/s. This has the further advantage that eruptions or eruption phases with very high effusion rates ($\sim 10^3$ m^3/s) typically last only hours, while less intense eruptions can be expected to remain active and thus detectable for tens of days.

Present day volcanic resurfacing rates can be constrained by direct observation of new flows from repeat SAR imaging. Although it is dangerous to extrapolate from a data set

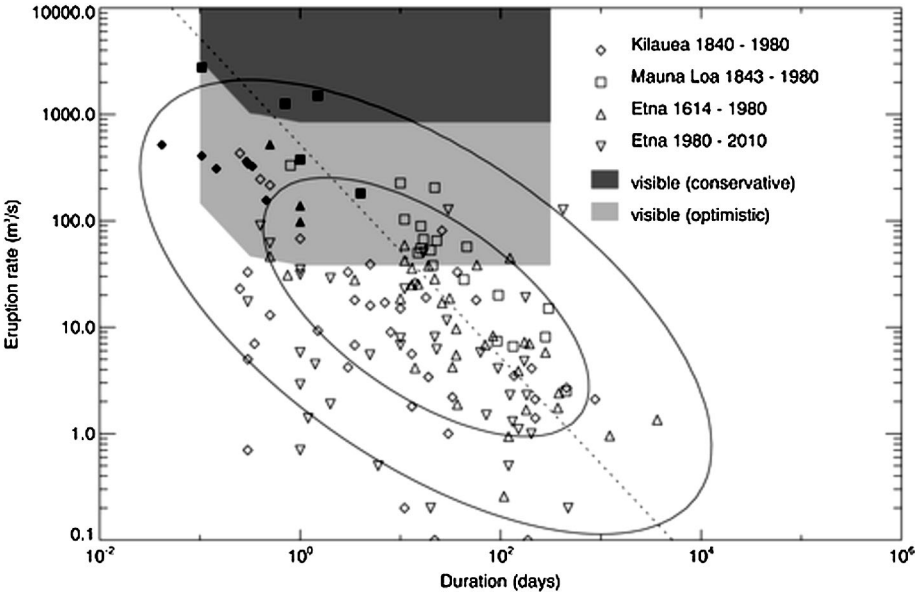

Fig. 8 From Mueller et al. (2017). Historical eruptions of three terrestrial volcanos from the data collated by Wadge [1981] and after 1980 by Harris et al. [2011]. Filled symbols represent only the initial phase of a few of the most intense eruptions. Grey areas indicate combinations of effusion rate and eruption duration that would be detectable by VIRTIS under the optimistic and conservative sets of assumptions. The solid lines correspond to isolines of a fitted probability density function that encompass 95% and 68% of eruptions. The dotted line corresponds to a volume of 0.045 km^3

of one, the observation of change during the Magellan mission by Herrick and Hensley (2023) indicates that it is almost certain that future missions will see changes from volcanism (new flows and structures) since Magellan and during their missions. When combined with various analyses attempting to extrapolate from terrestrial observations (Lorenz 2015; Byrne and Krishnamoorthy 2022a,b; van Zelst 2022), it seems likely that somewhere between a few to several dozen detectable volcanic eruptions occur on Venus in an Earth year.

8 Other Geologic Constraints

Here we consider a few other sets of geologic features whose nature and location bear upon the resurfacing and climate history of Venus. First, we examine the abundance and orientation of wrinkle ridges, a tectonic feature that occurs across most of the planet. We look at the possibility that the timing of formation of wrinkle ridges and polygonal structures may be related to climatic conditions. Then we consider the Venusian canali, a family of extremely long channels, each of which presumably formed over a short time period and can be used as a stratigraphic markers.

The geologic features known as "wrinkle ridges" represent limited contraction on coherent, layered surfaces such as lava plains and are found on multiple planets, including the Moon, Mercury, Venus, and Mars. On Venus, wrinkle ridges are ubiquitous in regional plains units. Efforts at mapping the orientations of wrinkle ridges demonstrated that they are associated predominantly with low elevations and low geoid values. Their strikes are generally perpendicular to both the local topographic slope and the local geoid slope (Bilotti

and Suppe 1999; Sandwell et al. 1997), suggesting that convection-driven topography creates sufficient stress to cause wrinkle-ridge formation perpendicular to the direction of flow from mantle upwelling to downwelling. As discussed in more detail in other articles of this collection, the general correlation of the geoid with the current distribution of large volcanoes and rifts makes a compelling argument that the overall mantle convection pattern has not reoriented during the period reflected in the visible geologic record. However, two of the stratigraphically youngest areas on the planet, with high geoid values, Beta and Atla Regiones, are notable for not being ringed by wrinkle ridges that strike perpendicular to their topography (Bilotti and Suppe 1999). An interpretation could be that these areas were uplifted after some internal or surface change (e.g. volcanic resurfacing) occurred that globally inhibits wrinkle ridge formation.

Climate models of a possible massive resurfacing event predict very substantial (several 100 C°) surface temperature excursions (Bullock and Grinspoon 2001), capable of producing tectonic deformation and a global stratigraphic marker. If such major temperature variations occurred, two studies predicted surface extension and contraction due to propagation of thermal waves due to climate change into the interior (Anderson and Smrekar 1999; Solomon et al. 1999). Climate-driven thermal stresses using a continuous plate predict that extension will produce polygons resembling hexagonal cooling of lava flows (Johnson and Sandwell 1992), but on a much larger scale due to the duration of the temperature excursion (Anderson and Smrekar 1999). A continuous plate model does not permit wrinkle ridge formation based on the Bullock and Grinspoon DT estimates. Solomon et al. (1999) assume a broken plate model, similar to what is used to model mid-ocean ridges, and predict both wrinkle ridges and polygons. Polygons occur in over 200 locations (Smrekar et al. 2002). Although wrinkle ridges can be produced by topographic slope, climate-change is the likely explanation for the observed sizes of polygons (up to several kms across). However, the apparent size of polygons observed in Magellan data may be under-resolved (Smrekar et al. 2002). Smaller diameter polygons could be a result of cooling lava flows. Future missions can test between these two hypotheses.

Magellan revealed a variety of channel and valley landforms, all of which likely transported lava and not water (Baker et al. 1992). Of particular interest are the 50 or so “canali”, channels that transported lavas hundreds of kilometers; the longest of these, Baltis Vallis, extends 6800 km (Baker et al. 1992; Komatsu et al. 1993). These features were each likely emplaced over relatively short periods of time (Komatsu et al. 1992) and thus represent time-stratigraphic markers that span long distances. Several of these features have topographic profiles that require post-emplacement regional tectonic warping (Komatsu and Baker 1994), and some of them have also experienced limited disruption by tectonic features such as wrinkle ridges. However, there are not clear instances where a canali has been cut by flows from a new shield volcano or other major later volcanism. An extensive mapping study of Baltis Vallis relative to its surroundings has been used as supporting evidence for the idea that the global stratigraphic sequence described above is also globally synchronous (Basilevsky and Head 1996).

9 Summary and Conclusions

The lack of small craters due to atmospheric filtering and the challenges of calibrating the cratering record in the last billion years means that there will likely always be ambiguity about the absolute timeline of the surface record for Venus, but Venus is clearly much closer to Earth than Mars in terms of its overall youthfulness. Upcoming missions (see Widemann

et al. 2023, this collection) will help constrain the timeline by 1) determining the level of current volcanic and tectonic activity through various monitoring approaches, 2) elucidating the details of how the impact craters have been altered post-impact with higher resolution imaging and topography, and 3) providing vastly improved imaging that will enhance our ability to separate lava flows and characterize key geologic contacts. Although the evidence suggests that most impact craters have experienced some post-impact volcanic modification, the current state of observations also allows one to interpret that as resulting from the final death knells of a "directional" resurfacing; in that case the near-random appearing spatial distribution of craters would largely represent a production surface. Resurfacing modeling can only produce a highly active present-day Venus with few altered craters in a near-random spatial distribution if resurfacing occurs in physically unrealistic ways that do not match the current geology.

However, to the extent that some or most of the craters are viewed as part of a continuum of features in various stages of being eliminated by volcanic and tectonic processes, then many more models become acceptable for creating a spatially near-random crater distribution. In this scenario, because the distribution of geologic terrain types (e.g., tessera, rifts, plains) is less random than the distribution of craters, there will have to be distinctly different mechanisms for removing craters in different regions that operate at somewhat similar rates.

Tying crater resurfacing to global views of the geologic history, the viewpoint that there is a global stratigraphy that shows a change in the nature of geologic activity and a rapid decline in the level of volcanism relies on a variety of assumptions, some of which will be testable with higher resolution imaging. Conversely, having different regions of Venus evolving independently of each other will require understanding how areally extensive features are maintained; for example, why there is a near-global wrinkle-ridge pattern that follows the current topography or why there are no volcanic flows that superpose canali. The improved resolution from future missions should better constrain how rapidly the vast volcanic plains were emplaced, the size and nature of individual flow events that emplaced those plains, and the timing of volcanism and deformation. Study of key geologic contacts, such as those between tessera units and embaying plains units, will be crucial in understanding the overall global geologic sequence.

Whatever "world view" of the geologic history that one develops from the new data from upcoming missions, its endpoint will have to be consistent with the constraints of where and how volcanism and tectonics are currently occurring.

Funding Note Open access funding provided by University of Oslo (incl Oslo University Hospital).

Declarations

Competing Interests The authors declare no competing interests relevant to this manuscript.

References

Airey MW, Mather TA, Pyle DM, Glaze LS, Ghail RC, Wilson CF (2015) Planet Space Sci 113:33
Anderson FS, Smrekar SE (1999) J Geophys Res, Planets 104:30743
Armann M, Tackley PJ (2012) J Geophys Res, Planets 117:E12003
Baker VR, Komatsu G, Parker TJ, Gulick VC, Kargel JS, Lewis JS (1992) J Geophys Res, Planets 97:13421
Basilevsky AT, Head JW III (1998) J Geophys Res, Planets 103:8531
Basilevsky AT, Head JW (1994) Earth Moon Planets 66:285
Basilevsky AT, Head JW (1995) Planet Space Sci 43:1523
Basilevsky AT, Head JW (1996) Geophys Res Lett 23:1497
Basilevsky AT, Head JW (2000) Planet Space Sci 48:75
Basilevsky AT, Head JW (2002) Geology 30:1015
Basilevsky AT, Head JW, Abdrakhimov AM (2004) J Geophys Res, Planets 109:E12003
Basilevsky AT, Shalygin EV, Titov DV, Markiewicz WJ, Scholten F, Roatsch T, Kreslavsky MA, Moroz LV, Ignatiev NI, Fiethe B (2012) Icarus 217:434
Bilotti F, Suppe J (1999) Icarus 139:137
Bjonnes EE, Hansen VL, James B, Swenson JB (2012) Icarus 217:451
Bondarenko NV, Head JW, Ivanov MA (2010) Geophys Res Lett 37:L23202
Brackett RA, Fegley B Jr, Arvidson RE (1995) J Geophys Res, Planets 100:1553
Brossier JF, Gilmore MS, Toner K (2020) Icarus 343:113693
Brossier J, Gilmore MS, Toner K, Stein AJ (2021) J Geophys Res, Planets 126:e2020JE006722
Brossier J, Gilmore MS, Head JW (2022) Geophys Res Lett 49:e2022GL099765
Bruno BC, Taylor GJ, Rowland SK, Lucey PG, Self S (1992) Geophys Res Lett 19:305
Bullock MA, Grinspoon DH (2001) Icarus 150:19
Bullock MA, Grinspoon DH, Head JW III (1993) Geophys Res Lett 20:2147
Byrne PK, Krishnamoorthy S (2022a) J Geophys Res, Planets 127:e2021JE007040
Byrne PK, Krishnamoorthy S (2022b) J Geophys Res, Planets 127:e2022JE007666
Campbell BA, Campbell DB (1992) J Geophys Res, Planets 97:16293
Campbell DB, Stacy NJS, Newman WI, Arvidson RE, Jones EM, Musser GS, Roper AY, Schaller C (1992) J Geophys Res, Planets 97:16249
Campbell BA, Morgan GA, Whitten JL, Carter LM, Glaze LS, Campbell DB (2017) J Geophys Res, Planets 122:1580
Carlson RW, Baines KH, Encrenaz T, Taylor FW, Drossart P, Kamp LW, Pollack JB, Lellouch E, Collard AD, Calcutt SB (1991) Science 253:1541
Carter et al (2023) Space Sci Rev 219
D'Incecco P, Müller N, Helbert J, D'Amore M (2017) Planet Space Sci 136:25
Dyar MD, Helbert J, Maturilli A, Müller NT, Kappel D (2020) Geophys Res Lett 47:e2020GL090497
Dyar MD, Helbert J, Cooper RF, Sklute EC, Maturilli A, Mueller NT, Kappel D, Smrekar SE (2021) Icarus 358:114139
Ekonomov AP, Golovin YM, Moshkin BE (1980) Icarus 41:65
Erard S, Drossart P, Piccioni G (2009) J Geophys Res, Planets 114:E00B27
Ernst RE, Head JW, Parfitt E, Grosfils E, Wilson L (1995) Earth-Sci Rev 39:1
Ernst RE, Grosfils EB, Mege D (2001) Annu Rev Earth Planet Sci 29:489
Ernst RE, Desnoyers DW, Head JW, Grosfils EB (2003) Icarus 164:282
Fegley B Jr (1997) Icarus 128:474
Fegley B Jr, Klingelhöfer G, Lodders K, Widemann T (1997) In: Bougher SW et al (eds) Venus II: Geology, geophysics, atmosphere, and solar wind environment, p 591
Filiberto J, Trang D, Treiman AH, Gilmore MS (2020) Sci Adv 6:eaax7445
Ganesh I, McGuire LA, Carter LM (2021) J Geophys Res, Planets 126:e2021JE006943
Garvin JB, Head JW, Zuber MT, Helfenstein P (1984) J Geophys Res, Solid Earth 89:3381
Gillmann C, Tackley P (2014) J Geophys Res, Planets 119:1189
Gilmore MS, Head JW (2000) Meteorit Planet Sci 35:667
Gilmore MS, Head JW (2018) Planet Space Sci 154:5
Guest JE, Stofan ER (1999) Icarus 139:55
Hansen VL (2000) Earth Planet Sci Lett 176:527
Harris AJ, Blake S, Rothery DA, Stevens NF (1997) J Geophys Res, Solid Earth 102:7985
Hashimoto GL, Imamura T (2001) Icarus 154:239
Hashimoto GL, Sugita S (2003) J Geophys Res, Planets 108:5109
Hauck SA, Phillips RJ, Price MH (1998) J Geophys Res, Planets 103:13635
Helbert J, Müller N, Kostama P, Marinangeli L, Piccioni G, Drossart P (2008) Geophys Res Lett 35:L11201
Helbert J, Maturilli A, Dyar MD, Alemanno G (2021) Sci Adv 7:eaba9428

Herrick RR (1994) Geology 22:703
Herrick RR, Hensley S (2023) Science 379:1205–1208
Herrick RR, Phillips RJ (1994a) Icarus 111:387
Herrick RR, Phillips RJ (1994b) Icarus 112:253
Herrick RR, Rumpf ME (2011) J Geophys Res, Planets 116:E02004
Herrick RR, Sharpton VL (1996) Geology 24:11
Herrick RR, Sharpton VL (2000) J Geophys Res, Planets 105:20245
Herrick R, Sharpton V, Malin M, Lyons S, Feely K (1997) In: Bougher SW et al (eds) Venus II: Geology, geophysics, atmosphere, and solar wind environment, p 1015
Ivanov M, Head JW (2001a) Geologic map of the Lavinia Planitia quadrangle (V-55), Venus. US Geological Survey Geologic Investigations Series I-2684
Ivanov MA, Head JW (2001b) J Geophys Res, Planets 106:17515
Ivanov MA, Head JW (2010) Planet Space Sci 58:1880
Ivanov MA, Head JW (2011) Planet Space Sci 59:1559
Ivanov MA, Head JW (2015) Planet Space Sci 106:116
Ivanov MA, Head JW (2004) Geologic Map of the Atalanta Planitia Quadrangle (V-4), Venus. US Department of the Interior, US Geological Survey
Ivanov MA, Head JW (2005) Geologic Map of the Nemesis Tesserae Quadrangle, V-13, Venus. US Department of the Interior, US Geological Survey
Ivanov MA, Head JW (2006) Geologic Map of the Mylitta Fluctus Quadrangle (V-61), Venus. US Geological Survey
Ivanov MA, Head JW (2008) Geologic Map of the Meskhent Tessera Quadrangle (V-3), Venus. US Department of the Interior, US Geological Survey
Ivanov BA, Basilevsky AT, Kryuchkov VP, Chernaya IM (1986) J Geophys Res, Solid Earth 91:413
Ivanov M, Head JW, Ryan DA (2010) Geologic map of the Lakshmi Planum quadrangle (V-7), Venus. US Department of the Interior, US Geological Survey
Iwagami N, Takagi S, Ohtsuki S, Ueno M, Uemizu K, Satoh T, Sakanoi T, Hashimoto GL (2011) Earth Planets Space 63:487
Izenberg NR, Arvidson RE, Phillips RJ (1994) Geophys Res Lett 21:289
Johnson CL, Sandwell DT (1992) J Geophys Res, Planets 97:13601
Kappel D, Haus R, Arnold G (2015) Planet Space Sci 113:49
Kappel D, Arnold G, Haus R (2016) Icarus 265:42
Karlsson R, Cheng KW, Crameri F, Rolf T, Uppalapati S, Werner SC (2020) J Geophys Res, Planets 125:e2019JE006340
King SD (2018) J Geophys Res, Planets 123:1041
Klose KB, Wood JA, Hashimoto A (1992) J Geophys Res, Planets 97:16353
Komatsu G, Baker VR (1994) Icarus 110:275
Komatsu G, Kargel JS, Baker VR (1992) Geophys Res Lett 19:1415
Komatsu G, Baker VR, Gulick VC, Parker TJ (1993) Icarus 102:1
Korycansky DG, Zahnle KJ (2005) Planet Space Sci 53:695
Kratter KM, Carter LM, Campbell DB (2007) J Geophys Res, Planets 112:E04008
Kreslavsky MA, Ivanov MA, Head JW (2015) Icarus 250:438
Labrosse S, Jaupart C (2007) Earth Planet Sci Lett 260:465
Le Feuvre M, Wieczorek MA (2011) Icarus 214:1
Lorenz RD (2015) Planet Space Sci 117:356
Lorenz RD, Le Gall A, Janssen MA (2016) Icarus 270:30
Lourenço DL, Rozel AB, Ballmer MD, Tackley PJ (2020) Geochem Geophys Geosyst 21:e2019GC008756
MacKenzie SM, Lorenz RD (2020) Remote Sens 12:2544
McKinnon WB, Zahnle KJ, Ivanov BA, Melosh HJ (1997) In: Bougher SW et al (eds) Venus II: Geology, geophysics, atmosphere, and solar wind environment, p 969
Mueller N, Helbert J, Hashimoto GL, Tsang CCC, Erard S, Piccioni G, Drossart P (2008) J Geophys Res Planets 113:E00B17
Mueller NT, Smrekar S, Helbert J, Stofan E, Piccioni G, Drossart P (2017) J Geophys Res, Planets 122:1021
Mueller NT, Smrekar SE, Tsang CCC (2020) Icarus 335:113400
Noack L, Breuer D, Spohn T (2012) Icarus 217:484
O'Rourke JG, Wolf AS, Ehlmann BL (2014) Geophys Res Lett 41:8252
Parmentier EM, Hess PC (1992) Geophys Res Lett 19:2015
Pettengill GH, Ford PG, Wilt RJ (1992) J Geophys Res, Planets 97:13091
Phillips RJ, Arvidson RE, Boyce JM, Campbell DB, Guest JE, Schaber GG, Soderblom LA (1991) Science 252:288

Phillips RJ, Raubertas RF, Arvidson RE, Sarkar IC, Herrick RR, Izenberg N, Grimm RE (1992) J Geophys Res, Planets 97:15923
Piccioni G, Drossart P, Suetta E, Cosi M, Amannito E, Barbis A, Berlin R, Bocaccini A, Bonello G, Bouyé M (2007) ESA Spec Publ, vol 1295. ESA, Noordwijk
Price M, Suppe J (1994) Nature 372:756
Price M, Suppe J (1995) Earth Moon Planets 71:99
Price MH, Watson G, Suppe J, Brankman C (1996) J Geophys Res, Planets 101:4657
Robinson CA, Wood JA (1993) Icarus 102:26
Rolf T, Steinberger B, Sruthi U, Werner SC (2018) Icarus 313:107
Rolf T, Weller M, Gülcher A, Byrne P, O'Rourke JG, Herrick R, Bjonnes E, Davaille A, Ghail R, Gillmann C (2022) Space Sci Rev 218:70
Romeo I (2013) Planet Space Sci 87:157
Romeo I, Turcotte DL (2008) Earth Planet Sci Lett 276:85
Romeo I, Turcotte DL (2009) Icarus 203:13
Romeo I, Turcotte DL (2010) Planet Space Sci 58:1374
Sandwell DT, Johnson CL, Bilotti F, Suppe J (1997) Icarus 129:232
Schaber GG, Strom RG, Moore HJ, Soderblom LA, Kirk RL, Chadwick DJ, Dawson DD, Gaddis LR, Boyce JM, Russell J (1992) J Geophys Res, Planets 97:13257
Seiff A, Schofield JT, Kliore AJ, Taylor FW, Limaye SS, Revercomb HE, Sromovsky LA, Kerzhanovich VV, Moroz VI, Marov MY (1985) Adv Space Res 5:3
Shalygin EV, Basilevsky AT, Markiewicz WJ, Titov DV, Kreslavsky MA, Roatsch T (2012) Planet Space Sci 73:294
Shalygin EV, Markiewicz WJ, Basilevsky AT, Titov DV, Ignatiev NI, Head JW (2015) Geophys Res Lett 42:4762
Shepard MK, Arvidson RE, Brackett RA, Fegley B Jr (1994) Geophys Res Lett 21:469
Shoemaker EM, Hackman RJ (1962) In: Kopal Z, Mikhailov ZK (eds) The Moon. Academic Press, London and New York, pp 289–300
Shoemaker EM, Wolfe RF, Shoemaker CS (1991) In: Abstracts of the Lunar and Planetary Science Conference, vol 22, p 1253
Smrekar SE (1994) Icarus 112:2
Smrekar SE, Moreels P, Franklin BJ (2002) J Geophys Res, Planets 107:8
Smrekar SE, Stofan ER, Mueller N, Treiman A, Elkins-Tanton L, Helbert J, Piccioni G, Drossart P (2010) Science 328(5978):605–608
Solomon SC, Head JW (1982) J Geophys Res, Solid Earth 87:9236
Solomon SC, Head JW, Kaula WM, McKenzie D, Parsons B, Phillips RJ, Schubert G, Talwani M (1991) Science 252:297
Solomon SC, Bullock MA, Grinspoon DH (1999) Science 286:87
Stofan ER, Guest JE, Copp DL (2001) Icarus 152:75
Stofan ER, Smrekar SE, Mueller N, Helbert J (2016) Icarus 271:375
Stöffler D, Ryder G, Ivanov BA, Artemieva NA, Cintala MJ, Grieve RAF (2006) Rev Mineral Geochem 60:519
Stone PH (1975) J Atmos Sci 32:1005
Strom RG, Schaber GG, Dawson DD (1994) J Geophys Res, Planets 99:10899
Tauber ME, Kirk DB (1976) Icarus 28:351
Team VBS, Seiff A (1987) Adv Space Res 7:323
Turco RP, Toon OB, Park C, Whitten RC, Pollack JB, Noerdlinger P (1982) Icarus 50:1
Turcotte DL (1993) J Geophys Res, Planets 98:17061
Turcotte DL, Schubert G (2017) Geodynamics. Cambridge University Press, Cambridge
Uppalapati S, Rolf T, Crameri F, Werner SC (2020) J Geophys Res, Planets 125:e2019JE006258
van Zelst I (2022) J Geophys Res, Planets 127:e2022JE007448
Voigt JR, Hamilton CW, Steinbrügge G, Scheidt SP (2021) Bull Volcanol 83:1
Weller MB, Kiefer WS (2020) J Geophys Res, Planets 125:e2019JE005960
Wichman RW (1999) In: Lunar and Planetary Science XXX, p 1156
Widemann T et al (2023) Space Sci Rev 219
Wilhelms DE, McCauley JF, Trask NJ (1987) The geologic history of the Moon
Wilson et al (2023) Space Sci Rev 219
Wood JA (1997) Bougher SW et al (eds) Venus II: Geology, geophysics, atmosphere, and solar wind environment, p 637
Wood BE, Hess P, Lustig-Yaeger J, Gallagher B, Korwan D, Rich N, Stenborg G, Thernisien A, Qadri SN, Santiago F (2022) Geophys Res Lett 49:e2021GL096302
Wright R, Blake S, Harris AJ, Rothery DA (2001) Earth Planet Sci Lett 192:223

Wright R, Blackett M, Hill-Butler C (2015) Geophys Res Lett 42:282
Zolotov M, Volkov VP (1992) In: Barsukov VL et al (eds) Venus geology, geochemistry and geophysics. University of Arizona Press, Tucson, pp 177–199

Authors and Affiliations

Robert R. Herrick[1] · Evan T. Bjonnes[2] · Lynn M. Carter[3] · Taras Gerya[4] · Richard C. Ghail[5] · Cédric Gillmann[6,4] · Martha Gilmore[7] · Scott Hensley[8] · Mikhail A. Ivanov[9] · Noam R. Izenberg[10] · Nils T. Mueller[11] · Joseph G. O'Rourke[12] · Tobias Rolf[13,14] · Suzanne E. Smrekar[8] · Matthew B. Weller[2,15]

✉ T. Rolf
tobias.rolf@geo.uio.no

R.R. Herrick
rrherrick@alaska.edu

1 Geophysical Institute, University of Alaska Fairbanks, Fairbanks, 99775-7320, USA

2 The Lunar and Planetary Institute, 3600 Bay Area Blvd, Houston, TX 77058, USA

3 Lunar and Planetary Laboratory, University of Arizona, 1629 E. University Blvd, Tucson, AZ 85721, USA

4 Institute of Geophysics, ETH Zurich, NO H 9.2, Sonneggstrasse 5, 8092 Zürich, Switzerland

5 Department of Earth Sciences, Royal Holloway, University of London, Egham, Surrey, TW20 0EX, UK

6 Department of Earth, Environmental and Planetary Sciences, Rice University, MS-126, 6100 Main Street, Houston, TX 77005, USA

7 Dept. of Earth and Environmental Sciences, Wesleyan University, 265 Church St., Middletown, CT 06459, USA

8 Jet Propulsion Laboratory, California Institute of Technology, Pasadena, CA 91109, USA

9 Laboratory of Comparative Planetology, Vernadsky Institute of Geochemistry and Analytical Chemistry, Russian Academy of Science, 119991 Kosygin street, Moscow, Russia

10 Space Exploration Sector, Atmospheres and Ionospheres Group, Johns Hopkins University Applied Physics Laboratory, 11100 Johns Hopkins Road, Laurel, MD 20723, USA

11 Institute of Planetary Research – Department of Planetary Physics, German Aerospace Center (DLR e.V.), Rutherfordstr. 2, 12489 Berlin, Germany

12 School of Earth and Space Exploration, Arizona State University, Tempe, AZ, USA

13 Centre for Earth Evolution and Dynamics (CEED), University of Oslo, P.O. Box 1028 Blindern, 0315 Oslo, Norway

14 Institute for Geophysics, University of Münster, Corrensstraße 24, 48149 Münster, Germany

15 Department of Earth, Environmental and Planetary Sciences, Brown University, 324 Brook Street, Providence, RI 02912, USA